Integrated assessment of the hydraulic and structural performance of crown walls on top of smooth berms

Manuscript submitted to Coastal Engineering for re-review and possible publication

INTEGRATED ASSESSMENT OF THE HYDRAULIC AND STRUCTURAL PERFORMANCE OF CROWN WALLS ON TOP OF SMOOTH BERMS

Sara Mizar Formentin[1], Giuseppina Palma[1], Barbara Zanuttigh[1]

(1) Department of Civil, Chemical, Environmental and Materials Engineering, University of Bologna, Viale del Risorgimento 2, Bologna 40136, Italy.
saramizar.formentin2@unibo.it, giuseppina.palma2unibo.it, barbara.zanuttigh@unibo.it

Abstract

The introduction of crown walls with parapets on top of dikes and berms represents a relatively economic and efficient solution to reduce the wave overtopping discharge and therefore the hazard exposure of the inshore areas. However, the inclusion of parapets and bullnoses leads to increased wave pressures on the crown walls that may compromise their resistance. Literature studies have so far addressed separately the effects of crown walls, parapets and bullnoses on the hydraulic efficiency and on the structural stability. The purpose of this contribution is to fill the gap between these two streams of research, proposing an integrated analysis of the wave loads and of the wave overtopping discharges at smooth berms that are supposed to be upgraded with crown walls and parapets. The study is based on the results of a recent campaign of 2D small-scale laboratory tests on wave overtopping at smooth berms with crown walls under breaking and non-breaking waves. Relevant parameters of the sensitivity analysis are the berm slope, width and relative emergence, the crown wall height, and the inclusion of a parapet. The main outcome of the investigation consists of a set of indications for the optimized reduction of the discharge with a limited increase of structural loads. A simple and practical formula linking forces and overtopping discharges at walls and highlighting the strict correlation between the two variables is also proposed.

Keywords: wave overtopping; wave force; crown wall; parapet; wave breaking; small-scale experiments

Highlights

- 128 new experiments of wave overtopping and impacts at smooth berms with walls
- integrated hydraulic and structural performance of crown walls and parapets
- indications for a structurally safe and hydraulically efficient upgrade of dikes
- test and extension of existing formulae for the wave forces at crown walls
- new fitting of wave forces at crown walls on wave overtopping discharges

1. Introduction

The necessity and urgency of upgrading existing coastal defense structures to resist the increasing violence of storms events and to face higher sea levels due to climate change (inter alia: Nicholls, 2002; Woodruff et al., 2013) are highly topical issues to be addressed in the present and immediate future (Burcharth et al., 2018). Among other approaches (Touili et al., 2014; Zanuttigh et al., 2014a), the introduction of crown walls with parapets on existing dikes and/or berms might represent a relatively economic, aesthetic and efficient solution to reduce the wave overtopping discharge q without requiring significant works (Van Doorslaer et al., 2015; Zanuttigh and Formentin, 2018). However, several studies have already demonstrated that the use of sloping parapets or bullnoses might expose the structures to non-negligible increase of wave loads (Castellino et al., 2018; Martinelli et al., 2018) due to the impulsive pressures enhanced by the confined return flow. The increase of the loading induces extra failure paths, and the failure is more brittle (i.e. a swift failure occurs if the design load is reached compared to standard dikes which have a higher remaining strength after initial failure). So, the introduction of parapets or the extension of crown walls in design should be carefully considered and benefits/drawbacks weighed.

Wave loads on rubble mound breakwaters with crown walls were experimentally investigated by Pedersen (1996), Martin et al. (1999), Norgaard et al. (2013). Recently, some studies focused on the structural response of walls and parapets in case of smooth structures. Chen et al. (2015) performed a small-scale 2D laboratory campaign to analyze the overtopping flow loads induced by broken regular waves on smooth dikes with crown walls in presence of shallow foreshores. This research was extended with further irregular tests to characterize the statistical distribution of the extreme overtopping forces at the walls and identify the maximum wave force acting under a known storm peak duration (Chen et al., 2016). Van Doorslaer et al. (2015) tested at small-scale crown walls and parapets placed on smooth dikes under non-breaking waves. Van Doorslaer et al. (2017) conducted small-scale laboratory tests in different facilities, prompting the first design formula for predicting the wave forces on a crown wall in irregular non-breaking wave conditions. A refitting of such formula was then proposed by De Finis et al. (2020) based on experimentally-calibrated numerical tests on smooth dikes with various promenade lengths, wall heights and water depths under plunging and surging breaker waves. Formentin and Zanuttigh (2019) extended the database by Van Doorslaer et al. (2015) including breaking wave conditions and developing a more exhaustive formula, based on the genetic programming technique.

Few studies including contemporary measurements of overtopping discharges and hydraulic loads at walls are available from the literature. Pedersen (1996) collected the first database of experimental data on wave overtopping and wave forces on crown walls on top of mound breakwaters differently armored (rock, cube, and Dolos). Smolka et al. (2009) carried out a series of small-scale 2D tests against a cube- and Cubipod-armored mound breakwater in non-breaking conditions, measuring the data of the dimensionless horizontal and up-lift forces and of the overturning moments at the crown wall. Both these datasets were adopted by Molines et al. (2018) to get estimations of the wave forces and overturning moments on crown walls from

various parameters, including the dimensionless wave overtopping discharge. The work of Molines et al. (2018) highlighted for the first time the strict correlation between overtopping discharge and forces at the walls, prompting – with the support of an Artificial Neural Network – an earliest relationship linking the 2 variables each other. Van Doorslaer (2018) presented the results of both wave overtopping discharges and forces, simultaneously measured during the campaigns described in Van Doorslaer et al. (2015, 2017). Martinelli et al. (2018) conducted regular and irregular tests of wave overtopping against a seawall with a recurved parapet whose inclination angle ε was made varying between 0° and 90°. During the tests, which included non-breaking waves exclusively, measurements of the overtopping discharge and of the wave forces at the basis of the wall were collected.

The datasets by Pedersen (1996), Smolka et al. (2009), Van Doorslaer (2018) and Martinelli et al. (2018) enclose – to our knowledge – the only data available of contemporary measurements of overtopping discharges and forces. Nevertheless, in all these studies, the focus is the analysis of the wave loads and the data of q are either used as parameters for the characterization of the experiments with respect to the literature (Martinelli et al., 2018) or considered as "input data" to derive the wave forces (Molines et al., 2018). An integrated analysis of wave loads and overtopping discharges at crown walls, dedicated to the connection and unification of the results of separate researches and addressing the inconvenience that a solution that may improve the hydraulic efficiency might contemporary enhance the structural loads and vice versa, is missing.

The work we are proposing in this contribution starts from this finding, to analyze a different case: smooth berms that are supposed to be upgraded with the construction of a crown wall at the inshore edge and with the inclusion of a parapet on top of the crown wall. Our aim is to provide the first integrated and systematic analysis of the structural and hydraulic performance of this kind of structures under both breaking and non-breaking waves, including a sea-level rise scenario where the berms are barely emerging or even submerged. The selection of the structure configurations is meant to pursue and extend the work by Van Doorslaer et al. (2017) and De Finis et al. (2020), who conducted laboratory and numerical tests of wave overtopping against long and sloping promenades with a crown wall on top, subjected to non-breaking waves.

To our purpose, the results of the experimental tests recently carried out in the Hydraulic Laboratory of the University of Bologna against smooth berms have been analyzed to integrate the data on the wave overtopping discharge q (Zanuttigh and Formentin, 2018; Formentin and Zanuttigh, 2019) with the data on the wave loads (pressures p and forces F) at the crown walls (Formentin et al., 2019a) to conduct a parametric analysis of the effects of varying the basic smooth berm configuration through the introduction of the mentioned structural upgrades. Specific objectives of this study are: i) to individuate the combination of the structural upgrades that contemporarily ensure an efficient reduction of q and limit the increase of the wave impact; ii) to individuate the sections of the crown walls that are subjected to the highest stresses in terms of intensity and frequency of impact; iii) to test and extend the existing formulae for the prediction of the extreme wave forces F at the walls against the new experimental data; iv) to suggest a simple formula to derive F from q under these same geometrical and hydraulic conditions.

The contribution is organized as follows. Section 2 describes the laboratory facility and the experimental tests, illustrating the different tested configurations, the measurements and the equipment. Section 3 analyses the experimental results of q and compares them with recently developed formulae. The effectiveness of the structural upgrades on the reduction of q is also investigated. Section 4 is dedicated to the elaboration of the pressure signals at the crown walls, illustrating the frequency of wave impacts, the results of the statistical analysis of the pressure values and the parametric analysis of the pressure distributions along the crown walls. Section 5 presents the results on the extreme wave forces F acting at the walls in comparison with predicting formulae from the literature and proposes a new, simple formula to correlate wave loads and discharges allowing the direct calculation of F from q.

2. The experimental tests

2.1. Experimental setup and tested configurations

The experiments were conducted in the small wave flume of the Hydraulic Laboratory of the University of Bologna (Unibo), which is 12 m long, 0.5 m wide and 0.7 m deep. The wave-maker, which produces the waves by vertical movements under the control of the mass conservation law (Galvin, 1964; Wang, 1974), can generate significant wave heights H_s up to 0.07 m and maximum wave lengths of ≈3 m. The maximum water depth at the wave-maker is 0.45 m. The schematic layout of the wave flume is given in Figure 1a, while the details of the instruments installed across the channel and the structure cross-section are sketched in Figures 1b, 1c and 1d.

The structures consist of smooth berms, characterized by a “finite” horizontal berm width (B) with a crown wall deeply clamped in the dike at the inshore edge. In this “monolithic” structure, the water could not filter beneath the dike and sliding and overturning were prevented because the structural stability assessment was out of the scope of the analysis.

The geometry and size of these structures followed previous experimental works, specifically: the slopes ($\cot\alpha_d$), the berm elevation to the bottom of the channel (h_c) and the value of B=0.15 m were setup following Schüttrumpf and Oumeraci (2005), while the value of the crown wall height (h_w=0.04 m) was selected in the range set up by Van Doorslaer et al. (2015). Starting from this “basic configuration”, representing the benchmark case, the following structural upgrades were hypothesized: extension of B (+100%), extension of h_w (+25%), introduction of a sloping parapet. The setup of the upgrades followed the findings of the researches carried out by Van Doorslaer et al. (2015) and by Formentin and Zanuttigh (2019). The size and geometry of these structures may reproduce a typical prototype Dutch dike (see Jonkman et al., 2013) in scale 1:20 (as for the crest width) or 1:30 (as for the structure height). The scale 1:20 is indeed preferred to keep the reference to the tests by Schuttrumpf and Oumeraci (2005).

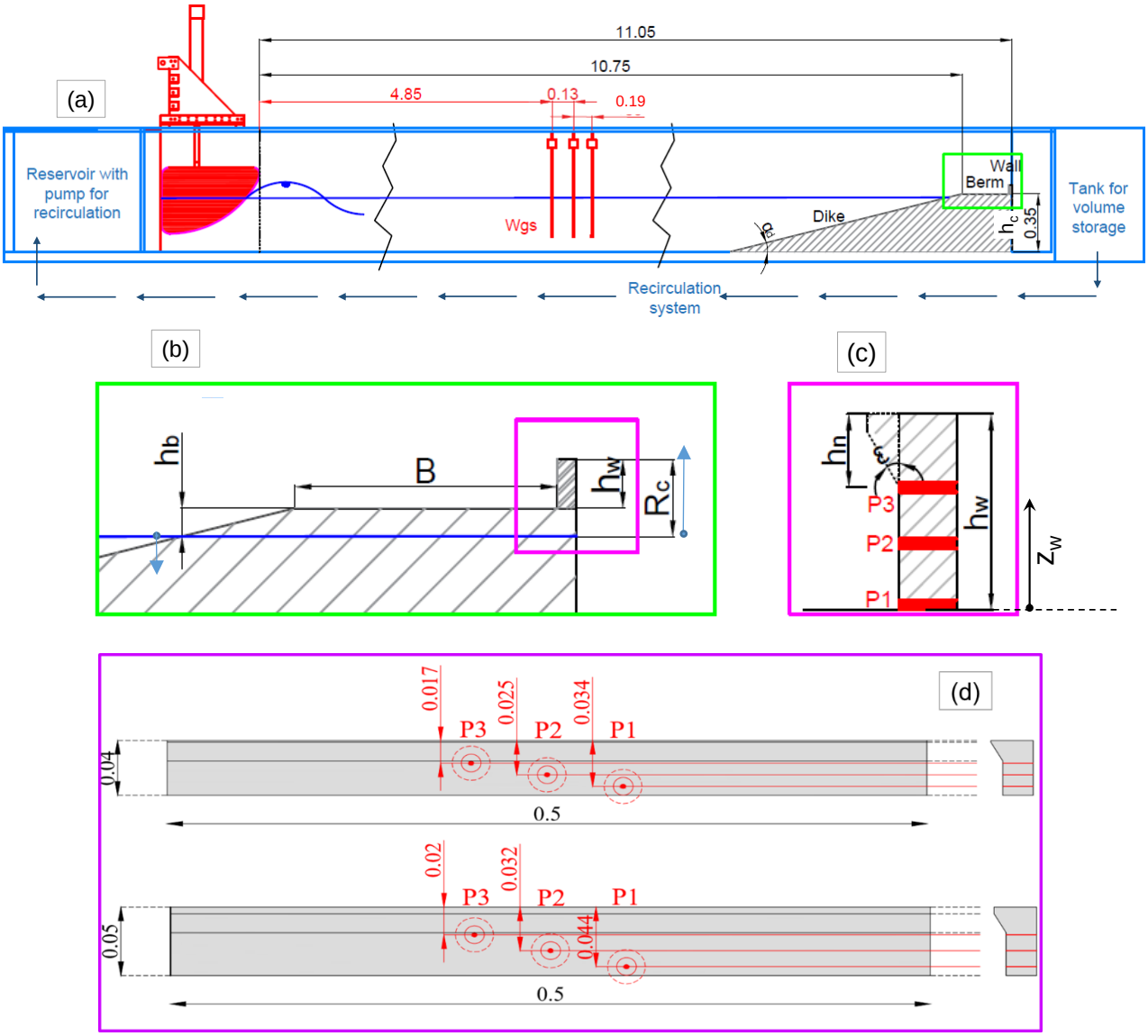

Figure 1. (a) Scheme of the wave flume of the hydraulic laboratory of Bologna with installation of the tested structures and instruments; (b) particular of the berm and crown wall; (c) particular of the crown wall with parapet and position of the pressure transducers (P1, P2, P3); (d) front and cross-sections of the 2 crown walls configurations (h_w=0.04 and 0.05 m) with reference to the position of the pressure transducers P1, P2 and P3. All the measures are in m.

Ultimately, the tested configurations at the lab model scale included: 2 offshore slopes cot(α_d)=2 or 4; 2 berm widths B= 0.15 and 0.30 m; 2 berm relative emergences: h_b/H_s=0 (i.e. berm in correspondence of the still water level), and h_b/H_s=-0.5 (i.e. emerged berm); 2 crown wall heights, h_w=0.04 and 0.05 m. Half of the tests were carried out against crown walls including a sloping parapet on top (i.e. parapet inclination angle ε=30°, parapet relative height $\lambda=h_n/h_w$=0.375, where h_n is the parapet height) and half without the parapet (ε=0° and λ=0). The size and the shape of the parapet were selected among the ones tested by Van Doorslaer et al. (2015) based on the work carried out by Zanuttigh and Formentin (2018), who individuated λ=0.375 and ε=30° as the

optimal configuration to get the minimum q. Larger values of ε would indeed lead to lower overtopping discharges but would contemporarily lead to higher loads since more water is retained by the storm wall. The modest values of the berm relative emergences h_b/H_s=-0.5 and 0 were specifically set up to investigate the hydraulic and structural response of the dikes under sea-level rise in a climate change scenario.

The Figures 1a and 1b show the typical cross-section of the berms, including the symbols used to describe the main structural parameters. The details and the parameters of the crown wall with the parapet are schematized in Figure 1c.

The elevation of the berm (h_c=0.35 m, at model scale) was kept constant with respect to the bottom of the channel. The different structures were positioned in the wave flume so that the berm off-shore edge resulted always at the same distance of 10.75 m from the wave maker (see Figure 1a). The water depth in front of the structure was the same at the wave maker, as no foreshore or toe was included. Both breaking and non-breaking waves were tested, with values of the Iribarren-Battjes breaker parameter $\xi_{m-1,0}=\tan(\alpha_d)/(s_{m-10})^{0.5}$ varying between 1.23 and 4.00.

By combining the different geometrical features ($\cot(\alpha_d)$, B, h_b/H_s, h_w, ε), 32 structure configurations were obtained. Each configuration was subjected to 4 wave attacks, realized by varying the significant wave height (H_s=0.05 and 0.06 m) and the spectral wave periods ($T_{m-1,0}$) to obtain 2 target wave steepnesses ($s_{m-1,0}$=0.03 and 0.04). All the experiments consisted of approximately 500 irregular waves, characterized by a Jonswap spectrum with a peak enhancement factor γ=3.3. The number of 500 waves was selected to allow for an accurate representation of wave overtopping after Romano et al. (2012). Part of the tests was repeated (1 randomly selected wave attack for each configuration, for a total of 32 repeated tests) to check the repeatability of the peak wave loads, as the wave impact process is even more stochastic than the wave overtopping and previous authors used indeed a minimum of 500 waves to assess the loads on harbor structures (500 waves were selected by Kisacik et al., 2012 while 1000 waves were adopted by Cuomo et al., 2010 and Van Doorslaer et al. 2017). In these new tests, a wave train of 1000 waves was generated and then the 500 wave window containing the maximum wave height was selected, by assuming that the maximum wave height leads to the maximum force on the crown wall.

Overall, 128 experiments were therefore performed without considering the repeated tests. The summary of the tested configurations is given in Table 1.

The ranges of the berm elevations (h_b=-0.6, -0.5 and 0 m at prototype scale – note that negative values of the water depth above the berm h_b denote the case of emerged berms, see EurOtop 2018) and of the total freeboards (R_c=-h_b+h_w=[0.8-1.6] m) are the result of the constraints imposed by: i) the definition of the 2 values of the relative emergence, h_b/H_s=-0.5 and 0, for the analysis of the sea-level rise scenario, ii) the definition of realistic and low-aesthetic impacting h_w-values (0.8 and 1 m), and iii) the facility limit of the wave generation H_s≤0.06 m (corresponding to 1.2 m at prototype scale). While the tested conditions do correspond to mild frequent waves in the Mediterranean Sea and are therefore far from the typical berm design conditions, they

nonetheless allow for a systematic parametric investigation of the structural and hydraulic response of the abovementioned geometrical upgrades.

The flat slope of the berm (0%) may slow or block the backward-directed water flow consequent to the wave impact. In case of relatively short waves and/or large berm widths (i.e. higher values of the ratio $B/L_{m-1,0}$), the residual water layer standing above the berm after an impact may interact with the next incoming wave. The Unibo experiments were characterized by values of $B/L_{m-1,0}$ in the range 0.07-0.27, i.e. $L_{m-1,0}$ was from ≈3.7 to 14 times B. This means that the shorter waves above the longer width ($L_{m-1,0}$≈3.7B) followed one another after at least twice the space necessary for a wave to travel back and forth on the berm (2B). This time slot should allow in most cases the complete drainage of the water above the berm between 2 consequent impacts. Though it was not possible to check each impact, the analysis of the video-records of the experiments seems to confirm this assumption, overall. However, a small residual water layer was actually observed for the following configurations: cot(α_d)=2, B=0.3 m, h_b/H_s=0, ε=30°, $s_{m-1,0}$=0.04 (8 tests). The role of such residual layer would require further investigation. Chen et al. (2015) suggested that a second incoming wave can "jump" over the reflective water layer and thus lead to higher impacts, both in value and in impact location on the wall. Palma et al. (2020) obtained instead a reduction of the force of the subsequent wave impact in presence of a residual layer, acting as a “water bag” and dissipating the incoming wave energy.

Table 1. Summary of the target conditions of the 128 experiments grouped by h_b/H_s. Values at model scale.

$\mathbf{h_b/H_s}$	0	-0.5
H_s [m]	0.05; 0.06	0.05; 0.06
$s_{m-1,0}$ [-]	0.03; 0.04	0.03; 0.04
cot(α_d) [-]	2; 4	2; 4
B [m]	0.15; 0.30	0.15; 0.30
h_w [-]	0.04; 0.05	0.04; 0.05
parapet (ε, λ)	no; yes (30°, 0.375)	no; yes (30°, 0.375)
#	64	64

2.2. Measurements and equipment

The experimental tests included measurements of: the average wave overtopping discharge (q), the instantaneous wave pressures at the crown walls (p) and the incident and reflected wave heights. These measurements were obtained through the installation of the following instruments in the wave flume:

- 5 resistive wave gauges placed, respectively: the first one at approximately half wave length ($0.5 \cdot L_{m-1,0}$) from the wave-maker to control the generated free-surface elevation; the following 3 (indicated in Figure 1a as “wgs”) at ≈$1.5 \cdot L_{m-1,0}$ to separate the incident and reflected waves based on Zelt and Skjelbreia (1992) methodology; the last one (Figure 1b) in correspondence of the mid-section of the berm width to measure the overtopping layer thickness. The sampling frequency of 100 Hz was selected for all the gauges. The values of the wave reflection coefficients range from 0.30 to 0.65 and agree with the values measured

for similar experiments on smooth structures with walls. The wave reflection coefficients for the same dikes without crown wall are reported in Formentin et al. (2019b) and show a good agreement with existing formulae and predictions by EurOtop (2018) Artificial Neural Network. The reflection analysis both of wave reflection coefficients and of wave spectra did not show significant effects of re-reflected waves. However the effect of re-reflections cannot be completely excluded, and therefore changes in wave grouping and phase differences of the re-reflected waves might still affect wave loading and overtopping.

- 3 pressure transducers installed at different positions along the crown wall (P1, P2 and P3 in Figures 1c and 1d) to measure the wave loads. The positions of P1, P2 and P3 are detailed in Figure 1d for the 2 wall heights configurations, h_w=0.04 and 0.05, and were kept the same for all the tests. Specifically, defining the ordinate elevation z_w along the wall height: P1 was placed at the basis of the wall (z_w=0), P3 in correspondence of the basis of the parapet (both in case the parapet is present or not, z_w=0.625·h_w) and P2 in the middle between P1 and P3 (z_w=0.313·h_w, see Figures 1c and 1d). The axes of the pressure transducers were perpendicular to the wall itself facing directly the incident waves. P2 was set in the mid front section of the wall, while P3 and P1 were placed to the left and to the right of P2 and as close as possible to the center (see Figure 1d, front sections), to avoid or reduce to a minimum the side effects induced by the walls of the wave flume (see Sub-section 2.3). The position of the upper P3 sensor at the transition between the straight part of the wall and the parapet does not allow to fully describe the pressures along the parapet but it anyway allows to capture the highest loads, which are expected to occur at its basis, due to the energy release of the wave run-up jet. The load on the parapet should be lower thanks to the water flowing back with its pressures and to the back velocity component. Such a behavior was observed by Ravindar and Siriam (2019) and Ravindar et al. (2021) in case of parapets on vertical walls for small and large air trap, while the maximum load on the parapet occurred above the transition in case of slightly breaking waves without air entrainment. In case of wall without parapet, the maximum loads are expected to occur either at P1 or at P2, and therefore the position of P3 does not affect the measurement of the maximum pressure.
  Each transducer was characterized by: sampling frequency of 1 kHz; range of measurement 70 to 700 mbar; accuracy ±0.04% of the full scale; external diameter of 25 mm, with internal diameter of 3 mm, which correspond to the exposed part on the wall, for the effective measurement of the pressures. The small scale of the tests did not allow the introduction of a larger number of transducers, which would provide a more accurate distribution of the vertical profile of the wave pressures (Hofland et al., 2010).
- A recirculation system composed by: a tank for the storage of the overtopping volumes situated behind the dike, a conduit linking the overtopping tank to a reservoir placed upstream the wave-maker, a pump and a flowmeter leading to a precision in the measure of q of approximately $1 \cdot 10^{-5}$ m^3/s.

To evaluate the stiffness and the eigenfrequencies of the pressure transducers and of the structures tested in the lab – in particular of the crown wall and parapet parts – the structures were subjected to a series of weak impulsive loads produced with a hammer. Following this methodology (Martinelli et al., 2018), eigenfrequencies of approximately 100-150 Hz were

measured. The wave impact frequencies i.e. the frequency between the maximum and average pressure peaks) resulted (at model scale) in the range 140-260 ms (see Section 4), very close to other experimental works, a.o. Kisacik et al. (2012). The structural eigenfrequencies were therefore sufficiently higher than the wave impact frequencies, so no resonance phenomenon is expected and no low-pass filtering of the pressure signals is needed (Van Doorslaer et al. 2015b; De Finis et al., 2020).

The instantaneous pressures values measured at P1, P2 and P3 were integrated along the wall height to obtain the instantaneous hydrodynamic forces, F. Both pressures and forces were treated as stochastic values, and the statistics were extracted: the maximum, the mean and the median (p_{max}, p_{mean} and p_{median}; F_{max}, F_{mean}, F_{median}) and the quantiles 100 and 250 (p_{100}, p_{250} and F_{100}, F_{250}). These quantiles were estimated as the average pressure or force value of the highest $N_{ow}/100$ and $N_{ow}/250$ impact events respectively, where N_{ow} is the number of overtopping waves at the offshore edge of the berm of the test time series. Following the literature (Cuomo et al., 2010), the quasi-hydrostatic pressures, $p_{h,q}$, were estimated through the p_{250} values (see Sub-section 4.3).

2.3. Scale and model effects

The laboratory tests were conducted in 1:20 scale with respect to a hypothetic prototype structure, adopting a Froude similarity law. The small scale and the modest wave heights generated in the wave flume (see Sub-section 2.1) might influence the measurements of q and p, which might result distorted if re-scaled to prototype. The adoption of the Froude law involves indeed the distortion of the ratios of other forces, such as inertia to surface tension (Weber number) and inertia to viscosity (Reynolds number), affecting several phenomena from the air entrapment to the water compressibility.

A distorted scaling of the surface tension can affect the dynamics and the type of the wave breaking (Stagonas et al. 2011). The surface tension increases with decreasing length scale and tends to inhibit the wave plunging for shorter waves (wave lengths L<4 m). A plunging breaker type at prototype scale might transform into a spilling breaker at model scale, with a reduction of the wave energy dissipation. More generally, less energetic or less frequent wave breaking might occur, determining consequently higher overtopping rates and higher loads at the small scale. Despite all the tests present values of L<4 m (0.9<L<3.30 m), fully-plunging wave breakers were observed and filmed systematically (see Formentin et al., 2019a).

A distorted representation of the fluid viscosity leads to lower Reynolds numbers and larger viscous forces (Lykke Andersen et al., 2011; Altomare and Gironella, 2014) in the model tests. The experiments are characterized by Reynolds numbers in the range $\approx 7 \cdot 10^3$-$5 \cdot 10^4$, which rescaled to prototype conditions correspond to Reynolds numbers in the range $\approx 5 \cdot 10^5$-$2 \cdot 10^6$. Overall, reduced Reynolds numbers might determine higher drag coefficients and consequently, smaller run-up heights and less overtopping at small scale (Lykke Andersen et al., 2011). However, the effects of increased drag forces to scale effects are more significant for rubble

mound structures than for smooth structures (Franco et al., 2009). Moreover, the potential reduction of q due to the increased drag forces would be partially balanced by the potential increase of q determined by the increased surface tension.

The small scale may also determine a smaller amount of air entrapment (Van Doorslaer et al., 2017). The reduced presence of air bubbles is expected to reduce the wave energy dissipation inducing higher run-up, higher overtopping rates and higher values of the forces at the crown walls. Though the presence of air bubbles was systematically observed during all the experiments, the effective rate of the air entrainment has not been quantified yet.

The analysis of the experimental tests indicates that the combined effects of the surface tension, of the flow viscosity and of the air entrapment is modest for non-breaking waves and is more evident for breaking waves. The average values of q follow the same trend of similar literature data in case of non-breaking waves (see Sub-section 3.2), and no bias is observed. In case of non-breaking waves, the forces are well approximated by existing formulae and assume values similar to literature data, while they show higher values than existing data for breaking waves (see Sub-section 5.2). However, the discrepancies among the new data of the forces, the literature data and the formulae may also be due to the differences in the tested conditions and in the parameters ranges, especially in case of the milder slope and breaking waves.

The experimental tests might be also affected by model effects, due to the limited width (0,5 m) of the wave flume, that might generate “side effects” causing distortions or asymmetries of the wave shape in the longshore direction propagation. Such asymmetries were not measured but were not even visually observed. To limit the influence of these effects, all the measurements were taken in the middle section of channel or as close as possible (see the position of the pressure transducers P1, P2 and P3 in Sub-section 2.2).

Overall due to the small scale the results require validation before they can be applied in design.

3. Reduction of the wave overtopping discharge

This Section presents the new experimental data of the average wave overtopping discharges q, by comparing them with literature formulae and literature data, in order to illustrate the range of the q-values and characterize the accuracy of the measurements, with specific attention to the scale and the model effects (Sub-section 3.1 and 3.2). A parametric analysis of the reducing effects on q of the introduction of the several structural upgrades (berm, crown wall and parapet) is proposed (Sub-section 3.3).

3.1. Literature overview

To our knowledge, three literature formulae are available so far to predict q in case of smooth structures with berm (or promenade), wall and parapet. All the methods propose a reduction factor γ to be included in different predicting equations of q at sloping structures. The first method

was developed by Van Doorslaer et al. (2015) for non-breaking waves only (i.e. for values of $\xi_{m-1,0}>2$) and was calibrated on a database of more than 600 laboratory tests specifically carried out to investigate the reducing effects of crown walls, promenades and parapets on q. This method consists in the introduction of the reduction factor γ^* in the following equation:

$$\frac{q}{\sqrt{gH_{m0}^3}}=0.2\cdot exp\left(-2.28\cdot\frac{R_c}{H_{m0}\cdot\gamma^*}\right),\ \xi_{m-1,0}>2. \quad (1)$$

This formula represents a refitting of the EurOtop (2007) prediction equation for q for non-breaking waves, where the original coefficient 2.6 has been replaced by the coefficient 2.28 to fit the experiments carried out by Van Doorslaer et al. (2015). The definition of γ^* varies according to the specific combination of elements (promenade, wall and parapet) present in the structural configuration (see Van Doorslaer et al., 2015). The EurOtop (2018) manual adopted the formulations of γ^* by Van Doorslaer et al. (2015) conceived for Eq. (1) to be directly applied in the new formula for non-breaking waves presented by Van der Meer and Bruce (2014):

$$\frac{q}{\sqrt{gH_{m0}^3}}=0.09\cdot exp\left(-\left(1.5\cdot\frac{R_c}{H_{m0}\cdot\gamma^*}\right)^{1.3}\right),\ \xi_{m-1,0}>2 \quad (2)$$

Following the EurOtop (2018) approach, Zanuttigh and Formentin (2018) proposed a new reduction factor γ^{**} to extend the original method by Van Doorslaer et al. (2015) to breaking waves. This factor was calibrated on an extended database including the experimental tests carried out at Unibo presented in this manuscript and a numerical dataset of similar tests and was conceived to be applied to the EurOtop (2018) predicting equations for q:

$$\frac{q}{\sqrt{gH_{m0}^3}}=\frac{0.023}{\sqrt{\tan\alpha_d}}\cdot\xi_{m-1,0}\cdot exp\left(-\left(2.7\cdot\frac{R_c}{\xi_{m-1,0}\cdot H_{m0}\cdot\gamma^{**}}\right)^{1.3}\right),\ \xi_{m-1,0}\leq 2,\quad \gamma^{**}=\frac{\gamma^*}{\tanh\left(\xi_{m-1,0}\right)} \quad (3a)$$

$$\frac{q}{\sqrt{gH_{m0}^3}}=0.09\cdot\exp\left(-\left(1.5\cdot\frac{R_c}{H_{m0}\cdot\gamma^{**}}\right)^{1.3}\right),\ \xi_{m-1,0}>2,\qquad \gamma^{**}=\frac{\gamma^*}{\tanh\left(\xi_{m-1,0}\right)} \quad (3b)$$

The reduction factor γ^{**} coincides with γ^* in case of non-breaking waves (because the denominator $\tanh(\xi_{m-1,0})$ goes to 1 when $\xi_{m-1,0}$ goes to $+\infty$, and in the practice when $\xi_{m-10}>2$) and accounts for wave breaking effect when $\xi_{m-1,0}<2$.

Formentin and Zanuttigh (2019) later developed a new reduction factor, γ^*_{GP}, based on the Genetic Programming technique and fitted on the available data (i.e. the database by Van Doorsaler et al. 2015 and the experimental and numerical data by Zanuttigh and Formentin, 2018). This third formula is still based on the EurOtop (2018) formulae for breaking and non-breaking waves:

$$\frac{q}{\sqrt{gH_{m0}^3}}=\frac{0.023}{\sqrt{\tan\alpha_d}}\cdot\xi_{m-1,0}\cdot exp\left(-\left(2.7\cdot\frac{R_c}{\xi_{m-1,0}\cdot H_{m0}\cdot\gamma^*_{GP}}\right)^{1.3}\right),\ \xi_{m-1,0}\leq 2 \quad (4a)$$

$$\frac{q}{\sqrt{gH_{m0}^3}} = 0.09 \cdot exp\left(-\left(1.5 \cdot \frac{R_c}{H_{m0} \cdot \gamma_{GP}^*}\right)^{1.3}\right), \quad \xi_{m-1,0} > 2, \tag{4b}$$

where

$$\gamma_{GP}^* = \left(\frac{0.93}{tanh\,(1.5 \cdot \xi_{m-1,0})}\right) - \left(0.30 \cdot tanh\left(\frac{B}{L_{m-1,0}}\right)\right) - \left(0.40 \cdot tanh\left(\frac{h_w}{R_c}\right)\right) \cdot -(0.15 \cdot \varepsilon_{rad}). \tag{4c}$$

The comparison among the measurements and the literature formulae can be found in Zanuttigh and Formentin (2018) and Formentin and Zanuttigh (2019).

The Artificial Neural Network (ANN) developed by the Authors (Zanuttigh et al., 2017; Formentin et al., 2018) was also applied to represent the structures with bullnoses and parapets, by proposing a specific correction to a few input data (Zanuttigh and Formentin, 2018). The equivalent crest freeboard $R_{c,eq}$ and the equivalent berm width B_{eq}

$$B_{eq} = B + 2 \cdot h_n^* \cdot tan(\varepsilon), \; R_{c,eq} = R_c - h_n^* + \frac{h_n^*}{cos(\varepsilon)}$$

should both reproduce the “longer” distance to be travelled by the incident waves along the parapet to overtop the wall. The parameters B, h_n, ε, R_c are defined in the schemes in Figure 2, panels b) and c). The overturning effect on the overtopping waves is reproduced by introducing the equivalent roughness factor $\gamma_{f,eq}$

$$\gamma_{f,eq} = \gamma_f - 0.1$$

where the value of 0.1 was calibrated on the basis of the available datasets, i.e. the dataset by Van Doorslaer et al. (2015) and these new data Unibo. Therefore the validity of these corrections to the input parameters is so far limited to smooth structures (γ_f = 1) exclusively.

3.2. Comparison with existing data

The new data of q of non-breaking and breaking waves are compared to the available ANN method and to the literature data in Figures 2a and 2b, respectively. The literature data are derived from the EurOtop (2018) database and correspond to the tests on smooth dikes with promenades, walls and parapets carried out by Van Doorslaer et al. (2015) under non-breaking waves. There are no similar data available for breaking waves. The ANN is selected among the available methods (Section 3.1) since the comparison of the data with the existing formulae was already presented in other papers (Zanuttigh and Formentin, 2018; Formentin and Zanuttigh, 2019) and the existing formulae include specific refitting based on this limited amount of data. The ANN instead was trained against a variety of datasets at different scales and the comparison among ANN predictions and data grouped by non-breaking and breaking waves was never analysed. Figure 2 shows that the new data of q: i) fall in the same range as the literature data for non-breaking waves (panel a) and show approximately the same accuracy (rmse=0.039 and 0.041 for the datasets of Van Doorslaer et al., 2015 and the Unibo data, respectively); ii) the

95% confidence bands (red dashed lines) associated to the predictions of the ANN for these new data are narrower than the 95% confidence bands (black dashed lines) associated to the optimal predictions of the ANN trained on the original EurOtop database (rmse=0.047); iii) the data are symmetrically distributed around the bisector line (continuous black line), showing no systematic scatter. Therefore, the new data of q seem not to present any specific model effect and any evident scale effect or bias.

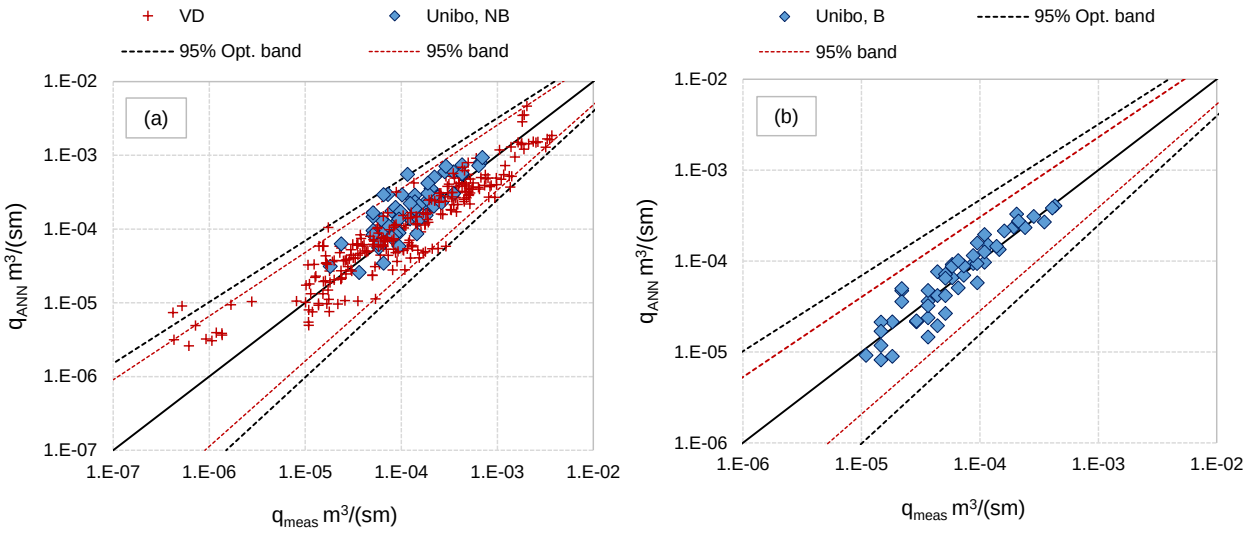

Figure 2. Comparison among the measured discharges q_{meas} and the predicted discharges by the ANN q_{ANN} for a) non-breaking ($\xi_{m\text{-}1,0}$>2) and b) breaking ($\xi_{m\text{-}1,0}$≤2) waves. The new data, Unibo, and the literature data by Van Doorslaer et al. (2015), VD, are plotted in panel a). The dashed red and black lines are the 95% confidence bands respectively for the ANN applied to Unibo and VD data and for the ANN optimal prediction associated to the original training database.

3.3. Effects of the structure geometry

The new collected database on q (Formentin and Zanuttigh, 2019) has been used to carry out a parametric analysis of the hydraulic effectiveness of the structural parameters to get a reduction of q, starting from the benchmark case of the "basic" configuration with no upgrades (B=0.15 m, h_w=0.04 m, ε=0°). Each of the following structural upgrades was separately investigated: i) the extension of the berm width B from 0.15 to 0.30 m; ii) the extension of the wall height h_w from 0.04 to 0.05 m; iii) the inclusion of the parapet with ε=30° (see Sub-section 2.1 and Table 1). The analysis of each upgrade was not correlated to the economic costs necessary to the installation of the upgrade itself. To assess the hydraulic effectiveness, the following parameter was defined:

$$Eff=(q_{basic}-q_{upgraded})/q_{basic}, \quad (5)$$

where q_{basic} and $q_{upgraded}$ are the values of q corresponding to the dike configuration respectively without and including one of the mentioned structural upgrades. The analyses were conducted considering the dimensionless quantity $q^*=q/(gH_sT_{m-1,0})$, which accounts for both the wave height and the wave period, based on the works by Hughes and Nadal (2009), and Zanuttigh et al. (2014b). The values of q_{basic}, $q_{upgraded}$ and *Eff* were calculated from the q^*-values.

The results of the analyses are summarized respectively in the Tables 2 and 3 for the tests with $\cot(\alpha_d)=4$, c4 in the following, and $\cot(\alpha_d)=2$, c2 in the following. This primary distinction reflects the separation into breaking and non-breaking waves suggested by EurOtop (2018) based on the values of $\xi_{m-1,0}$. Indeed, all the tests with c2 give $\xi_{m-1,0}>2$ while all the tests with c4 give $\xi_{m-1,0}\leq 2$. In both Tables 3 and 4 the results are organized as follows:

- the first column ("All data with c4" – or c2) reports the mean μ, the median and the maximum values of q^*, which were calculated on the whole group of tests with c4 or c2 (64 tests out of the whole database of 128 tests);
- in the next columns, the same statistics of q^* are given for the datasets extracted from the whole group by considering only the tests on structures without a specific upgrade (B=0.15 m, no parapet, or h_w=0.04 m) and with upgrade (B=0.30 m, parapet, or h_w=0.05 m); the couples of datasets relative to a specific upgrade (for example, B), include all the tests with or without that specific upgrade independently of the presence of the other upgrades (parapet, h_w);
- for each upgrade and for each statistics, the corresponding *Eff* parameter defined in Eq. (5) is reported (shaded columns);
- all the values of q^* are multiplied by 10^{-4}.

Table 2. Hydraulic effectiveness (*Eff*) of the structural upgrades and statistics of $q^*=q/(gH_sT_{m-1,0})$ for the group of breaking tests "c4". All the values of q^* are multiplied by 10^{-4}.

Statistics	**All data with c4** (#64)	**Extension of the berm width**			**Inclusion of the parapet**			**Extension of the wall height**		
	q^* x10^{-4}	q^* x10^{-4}		*Eff.*	q^* x10^{-4}		*Eff.*	*Eff.*		*Eff.*
		B=0.15	B=0.30		no	yes		h_w=0.04	h_w=0.05	
μ	**0.99**	1.22	0.76	37.7%	1.10	0.88	20.0%	1.40	0.59	57.9%
median	**0.64**	0.75	0.50	33.3%	0.67	0.50	25.4%	0.85	0.35	58.8%
max	**4.91**	4.91	3.27	33.4%	4.91	4.72	3.9%	4.91	2.37	51.7%

Table 3. Hydraulic effectiveness (*Eff*) of the structural upgrades and statistics of $q^*=q/(gH_sT_{m-1,0})$ for the group of non-breaking tests "c2". All the values of q^* are multiplied by 10^{-4}.

Statistics	**All data with c2 (**#64)	**Extension of the berm width**			**Inclusion of the parapet**			**Extension of the wall height**		
	q^* x10^{-4}	q^* x10^{-4}	q^* x10^{-4}	*Eff.*	Eff.	q^* x10^{-4}	*Eff.*	q^* x10^{-4}	q^* x10^{-4}	*Eff.*
		B=0.15	B=0.30		no	yes		h_w=0.04	h_w=0.05	
μ	**1.98**	2.18	1.79	17.9%	2.22	1.74	21.6%	2.69	1.28	52.4%
median	**1.57**	1.73	1.27	26.6%	1.77	1.07	39.5%	2.17	1.01	53.5%
max	**7.32**	7.32	5.60	23.5%	7.32	6.92	5.5%	7.32	4.84	33.9%

The effect of the wave breaking is paramount: the statistics of q^* obtained with c2 (Tab. 3) are approximately 2 times the statistics with c4 (Tab. 2). All the structural upgrades are more or less effective to reduce q. Generally, the more significant reductions are obtained on the mean and on the median values of q^*, with values of *Eff* ranging between ≈20-60%, while the reduction on the maximum q^* are more modest (*Eff* ≈5-50%). This suggests that, on average, the structural upgrades are more effective in case of medium-low rates of q^*. By looking at the results of the parametric analysis more in detail, the following considerations can be drawn.

- The most effective upgrade is represented by h_w, leading to a reduction of q^* of approximately the 50% (*Eff* =52-59% for c4 and *Eff* =34-54% for c2) in the face of rising h_w of the 25%. Differently from the other structural upgrades, h_w is effective to reduce also the maximum q^*-values, especially in case of breaking waves. The good effectiveness of h_w could be easily predicted, as the increase of h_w essentially corresponds to an increase of R_c.
- The upgrade of B and the inclusion of the parapet give similar performance (*Eff*≈20-40%), though B works better on the maximum q^*-values (*Eff*=24% and 33% for c2 and c4, respectively) with respect to the parapet (*Eff*=4% and 5% for c4 and c2).
- The effectiveness of the parapet as function of q^* is further investigated in Figure 3, which shows how *Eff* exponentially decreases from 70% to 0% with increasing q^* from ≈$2\cdot10^{-5}$ to ≈$7\cdot10^{-4}$. Similar trends are found for both the tests with c2 and with c4. The values of Tables 2 and 3 and Figure 3 suggest therefore that the inclusion of the parapet can be useful especially in case of relatively low overtopping rates, i.e. in combination with other structural upgrades. In a sea level rise scenario, where the berm level might be close to the still water level (h_b≈0, see Figure 1b), the inclusion of the parapet might lose effectiveness and result insufficient.
- The effectiveness of B is strictly related to the structure slope and to the occurrence of the wave breaking: while *Eff* varies between 33% and 37% in case of c4, i.e. when the waves break along the structure slope and reach the berm fully broken, it drops to 18-27% in case of c2, i.e. when the waves reach the berm unbroken. In the first case, the flow propagation along the berm width is affected by a non-negligible friction effect due to the high turbulence rate and due the presence of air entrainment (see Figure 4a). In such conditions, the longer the berm, the higher the dissipation rate and the lower the overtopping. On the contrary, when the wave breaking occurs just along the berm or directly in front of the wall (c2, see Figure 4b), the turbulence and the air entrainment are limited and the wave energy

dissipation is more modest. The different effect of B based on the occurrence of the wave breaking plays also a significant role in the characterization of the wave loads and on the assessment of the structural performance (see Sub-section 4.3.2).

- The berm width might represent an effective – though expensive – solution to reduce q, especially if considering that this study refers to smooth structures. The cost-effectiveness of this upgrade (doubling B gives the average Eff value of ≈30%) might improve significantly in case of permeable structures.

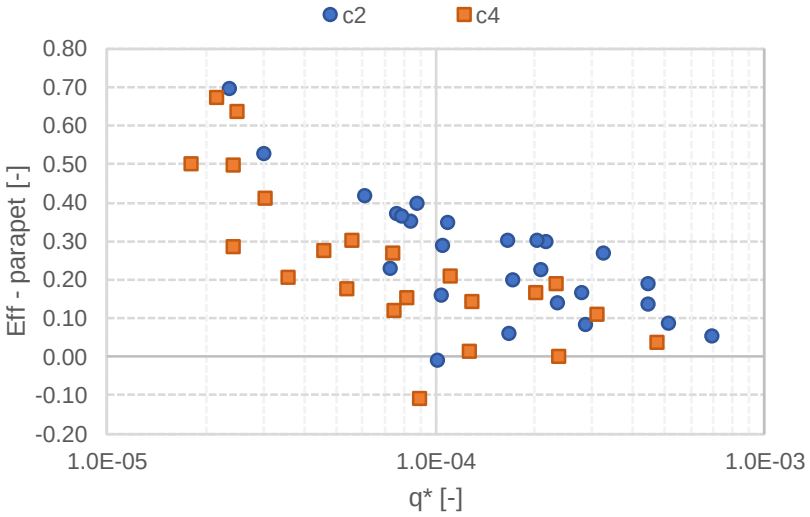

Figure 3. Hydraulic effectiveness (Eff) of the inclusion of the parapet to the reduction of the overtopping discharge as a function of the dimensionless values of $q^*=q/(gH_{m0}T_{m-1,0})$. Data grouped by cot(α_d).

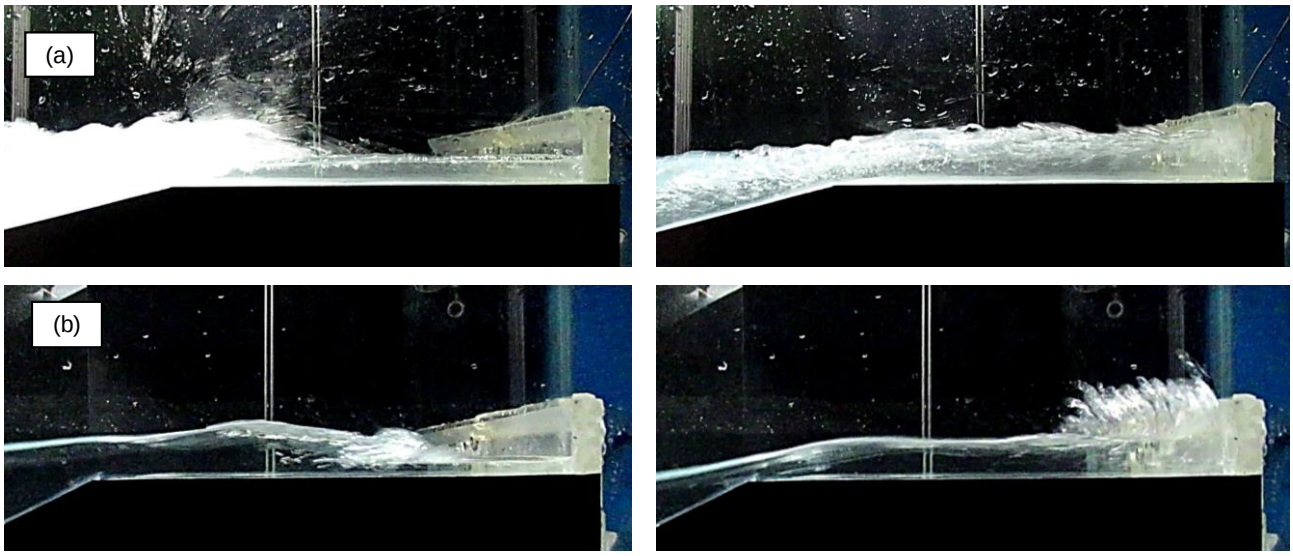

Figure 4. Consecutive frames of the same overtopping event (H_s=0.05 m, $s_{m-1,0}$=0.03) at the same structure (h_b/H_s=-0.5, B=0.30 m, h_w=0.5 m, parapet) characterized by cot(α_d)=4 (panel a) and cot(α_d)=2 (panel b). In the panel a, the wave breaks before the berm, while in the b the wave breaks just in front of the wall.

4. Analysis of the wave pressures

Starting from the preliminary analyses carried out by Formentin et al. (2019a), this Section presents the experimental results on the wave pressures (p) at the crown walls obtained from the experiments at Unibo. The number and the characterization of the wave impacts are illustrated in Sub-section 4.1, the distribution of the wave pressures in Sub-section 4.2 and the parametric analysis to the main geometrical parameters is given in Sub-section 4.3. A new procedure to extract the maximum and the quasi-hydrostatic peaks in the pressure signal has been developed and illustrated (Sub-sections 4.1 and 4.2).

4.1. Frequency of the wave impacts

The possibility to predict the number of the waves impacting against a crown wall for a given wave attack represents a key information for the assessment of the structural performance, resilience and fatigue resistance. The knowledge of the distribution of the number of the wave impacts along the wall height represents an additional information to assess the position of the wall more frequently subjected to the impacts.

To this purpose, the number of the wave impacts *Nimp* was calculated for each test and at each pressure transducer by elaborating the wave pressure signals with a built-in *Matlab* procedure that finds the local maxima in the pressure signals. This procedure was applied by defining the 2 following parameters: i) the minimum prominence value of p ($p_{min\ prominence}$); the term "prominence" comes directly from the *Matlab* syntax and refers to the minimum amplitude value that has to be exceeded, i.e. the minimum vertical amplitude of the p-signal to identify an "actual" impact event (instead than a small oscillation or noise) and ii) the minimum time-delay ($t_{min\ delay}$) that is expected to occur between two consecutive peaks. The calibration of these parameters was based on a trial-and-error process centered on the analysis of the statistical distribution of the p-values, on the values of the peak wave periods and on the visual examination of the wave signals. The final values of the parameters were set as follows: $p_{min\ prominence}=p_{100}/3$ Pa; $t_{min\ delay}=0.5$ s $\approx T_p/2$. Figure 5 gives an example of a pressure signal elaborated with the *Matlab* procedure with reference to the parameter $p_{min\ prominence}$ (triangles): in this figure, each wave impact identified is time-circumscribed by 2 consecutives down-crossings of $p_{min\ prominence}$. The circles represent the peaks of each impact event (p_{max}).

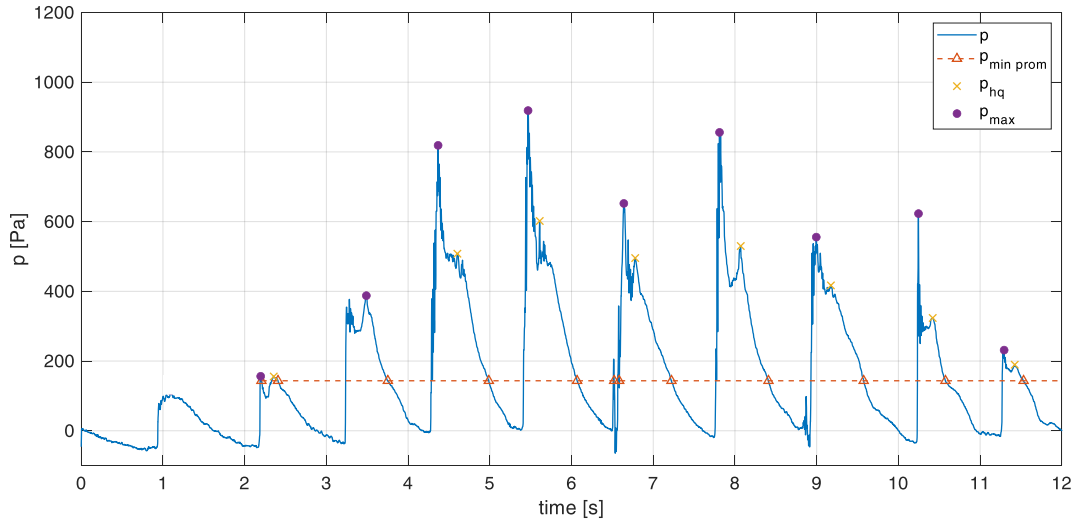

Figure 5. Example of a wave pressure signal (p) and reference to the parameters $p_{min\ prominence}$, p_{hq} and p_{max}.

The number of the wave impacts to the total number of overtopping waves, N_{imp}/N_{ow}, obtained for each test and each transducer, are charted in Figure 6 as a function of h_b/H_s. Van Doorslaer et al. (2017) proposed the following linear fitting of N_{imp}/N_{ow} vs h_b/H_s:

$$\frac{Nimp}{Now} = a \cdot \left(-\frac{h_b}{H_s}\right) + b, \tag{6}$$

where the values of the coefficients a and b are reported in Table 4 (first line). Note that the sign minus is included before h_b/H_s to account for the differ symbols adopted between the present work and the article by Van Doorslaer et al. (2017). The negative abscissas of Figure 6 are the result of the measured values of h_b/H_s instead of the target ones, which accounts also for the mean swl in the wave flume during the test. Specifically, h_b/H_s is <0 when the mean swl increases during the test, giving a slightly submerged berm condition. As it can be observed by the chart, the swl varied up to 5 mm, giving $h_b/H_s \approx -0.1$, maybe due to the small scale of the tests.

Table 4. Values of the coefficients a and b of Eq. (6).

Coefficients of Eq. (6)	***a***	***b***
Van Doorslaer et al. (2017)	-0.26	0.69
Fitting for P1	-0.23	0.59
Fitting for P2	-0.33	0.58
Fitting for P3	-0.33	0.48

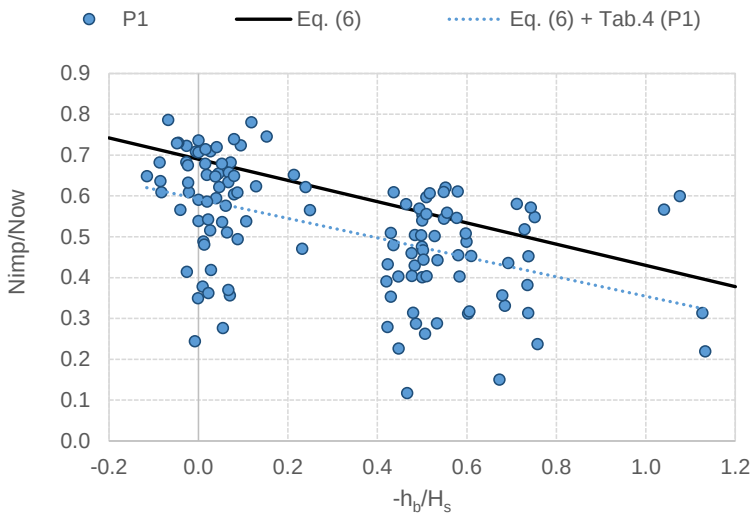

Figure 6. Relative number of wave impacts at P1 as a function of the berm relative emergence h_b/H_s. The lines represent the original fitting by Van Doorsaler et al. (2017), given by Eq. (6) (continuous) and the fitting of Eq. (6) with the coefficient optimized for the data at the transducer P1 (dashed) based on tab. 4.

The fitting by Van Doorslaer et al. (2017), which is targeted to estimate all the impacting waves at the basis of the wall, represents an upper envelope to most of the data, as it could be expected because of the non-zero distance of the lowest pressure sensor from the basis and because of the inclusion of the prominence amplitude in the elaborations. In line with this study, the *Nimp*/*Now* is always <1 and at maximum ≈0.8, even when h_b=0.

Actually, *Nimp*/*Now* varies significantly with the position of the pressure transducer, that is to say with the elevation along the wall height, z_w. To quantify the differences of the *Nimp*/*Now*-values at P1, P2 and P3, the average linear fittings of the 3 sets of data were derived. The resulting values of the coefficients *a* and *b* to be included in Eq. (6) to obtain the 3 different fittings are given in Table 4 (lines 2-4). The fitting line corresponding to the optimized fitting for P1 is plotted in Figure 6 as dashed line.

To further investigate the relationship between *Nimp*/*Now* and the position of the transducer along the wall height z_w, the statistics of *Nimp*/*Now* at P1, P2 and P3 were calculated on the whole dataset and the results are collected in Table 5. The statistics in this Table indicate that *Nimp*/*Now* decreases with z_w with an almost constant decrease rate from P1 (z_w=0, μ=0.52, max=0.79) to P2 (z_w=0.31·h_w, μ=0.47, max=0.78) and from P2 to P3 (z_w=0.625·h_w, μ=0.37, max=0.75), suggesting a linear relationship.

Table 5. Relative number of impact waves (*Nimp/Now*) at the pressure transducers P1, P2, P3.

Statistics	min	max	μ	σ
P1	0.12	0.79	0.52	0.15
P2	0.13	0.78	0.47	0.15
P3	0.05	0.75	0.37	0.16

Combining the existing relationship between *Nimp/Now* and h_b/H_s (Eq. 6) and the new information available from the data along the wall, z_w, the following new fit of the distribution of the impacts along the wall *Nimp_d* is proposed:

$$\frac{Nimp\_d}{Now} = \begin{cases} 0.65-0.3\cdot\frac{-h_b+z_w}{H_s}, \text{ for average prediction} \\ 0.83-0.3\cdot\frac{-h_b+z_w}{H_s}, \text{ for maximum envelope} \end{cases}. \quad (7)$$

The 2 different expressions for Eq. (7) provide, respectively, the average prediction and the maximum envelope of *Nimp_d/Now* along the wall height, for this new dataset, see Figure 7. The average and the maximum predictions can be used, respectively, as indication for the assessment of the frequency of the wave impacts in operating and design conditions. The parameter $(-h_b+z_w)/H_s$, varying between z_w=0 (basis of the wall) and $z_w=h_w$ (top of the wall), denotes the relative elevation of a point along the crown wall with respect to the still water level (swl). Giving a differentiated prediction of *Nimp_d* along the wall, Eq. (7) represents therefore an upgrade of Eq. (6). The scatter is still rather large, and therefore Eq. (7) may be used for individuating the most frequently stressed sections of the wall for a cautious assessment of fatigue effects at the wall, as well as Eq. (6). Note that the predictions by Eq. (7) should be considered as indicative due to the small scale of the tests. Further verification of Eq. (7) at larger scale experiments is recommended.

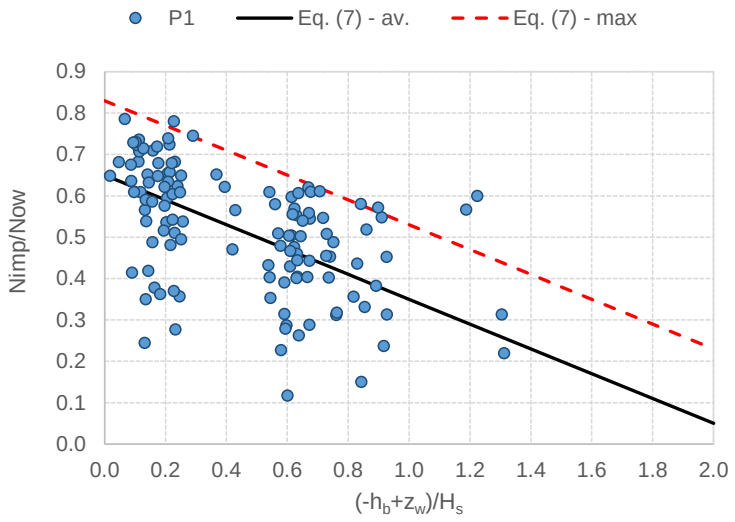

Figure 7. Relative number of wave impacts at P1 along the relative wall elevation to the swl, $(-h_b+z_w)/H_s$. The lines represent the curve of Eq. (7) giving an average prediction (continuous) and the upper envelope (dashed) of the data.

The σ-values reported in Table 5 quantify the scatter associated to the data and therefore the level of uncertainty associated to the predictions based on Eq. (7). Being σ=0.16 for all the transducers, the same dispersion and uncertainty level is obtained at each crown wall elevation.

A small effect of the berm width *B* on *Nimp/Now* was also observed, but negligible with respect to h_b and z_w. Though in the present study – focused on smooth structures – the parametrization of *Nimp_d/Now* against *B* was avoided, the relevance of *B* might become considerable in case of rough berms.

4.2. Characterization of the pressure signals

The pressure signals are here classified following the traditional methodology proposed by Oumeraci et al. (1993) and adopted by the PROVERBS project. This classification is based on the nature of the wave impacts and includes 4 different breaker types: i) slightly breaking waves, ii) impact loads, iii) broken waves and iv) quasi-standing waves. The determination of a specific breaker type depends on the combination of the wave characteristics and of the structure typology.

The type of structures most similar to the ones considered by the PROVERBS project is the crown walls rubble mound breakwater. For these structures, the slightly breaking waves (i) and the impact loads (ii) should be the recurrent types of wave impacts according to the PROVERBS map. Both these impact types present the typical “church spire” shape in the pressure signal, where the main pressure peak is followed by a trace of the duration of ~10^2 ms including a second, lower peak. The 2 peaks – which are evident in the example charts of Figure 8 – are respectively named p_{max} and $p_{h,q}$ and represent the maximum and the quasi-hydrostatic pressure values characterizing each wave impact. A specific range of values of the ratio $p_{max}/p_{h,q}$ is associated to each breaker type: $1<p_{max}/p_{h,q}<2.5$ for the slightly breaking waves (i) and $p_{max}/p_{h,q}>2.5$ for the impact loads (ii).

The values of p_{max} and $p_{h,q}$ have been calculated at each pressure transducer for each wave impact of each test. While the extraction of the p_{max}-values is relatively simple (see Sub-section 4.1), the automatic determination of the $p_{h,q}$-values subsequent to each maximum is not straightforward. To this purpose, the following procedure was followed:

1. The p_{max}-values were firstly individuated for each pressure signal (circles in Fig. 8) by means of the dedicated *Matlab* function (see Sub-section 4.1).
2. The time delay of $p_{h,q}$ after p_{max} depends on the duration of the pressure trace after the spike interval, which in turns depends on the nature of the wave impact itself and on the amount of air entrainment (Bullock et al., 2007; Plumerault et al., 2012). Bullock et al. (2007) found durations of such pressure trace after p_{max} (at model scale) of 80-200 ms and 100-450 ms for low-aeration and high-aeration wave impacts, respectively. Therefore the maximum time delay of 500 ms (at model scale) was cautiously chosen and its adequacy was verified by randomly examining some of the results.

3. The same *Matlab* function was applied to find the local maximum in each interval of 500 ms subsequent to p_{max}; the peaks returned by the function are the $p_{h,q}$-values. The parameter $p_{min\ prominence}$ was still set equal to $p_{100}/3$ Pa, while no value was assigned to $t_{\text{min delay}}$, as the delay between p_{max} and $p_{h,q}$ is not known *a priori* and varies for each impact.

The $p_{h,q}$-values obtained with this automatic procedure are indicated with crosses in Figure 8.

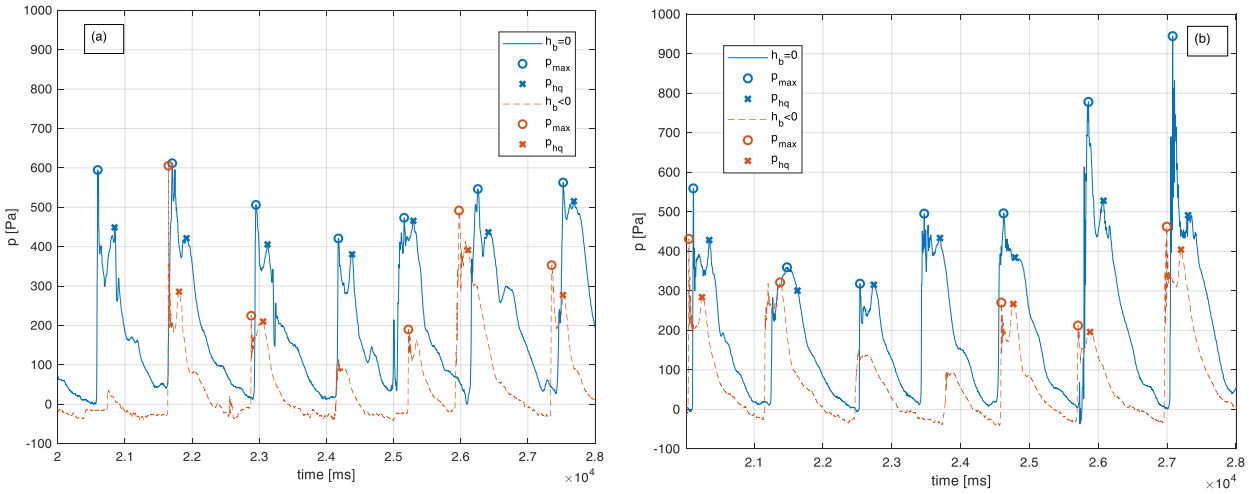

Figure 8. Example time series of the wave pressures (p) recorded at P1 during the same test (H_s=0.05 m, $s_{m\text{-}1,0}$=0.03, B=0.15 m, h_w=0.05 m) with emerged berm (h_b<0) and berm at the swl (h_b=0). Structure with $cot\alpha_d$=4 and $cot\alpha_d$=2 in panels (a) and (b), respectively.

For each wave impact, the ratio $p_{max}/p_{h,q}$ was calculated. For each test and each pressure transducer, the distribution of the $p_{max}/p_{h,q}$-values was analyzed by computing the frequency of occurrence of the impacts characterized by: i)$1<p_{max}/p_{h,q}<2.5$, ii) $p_{max}/p_{h,q}\geq 2.5$ and iii) $p_{max}/p_{h,q}\approx 1$.

When the value of $p_{h,q}$ is missing (i.e. when the function failed in the determination of the quasi-hydrostatic peak subsequent to a p_{max}-value) the whole impact event is discarded from the statistical analysis. On average, the percentage of missing $p_{h,q}$-values is limited to 2-3% for each pressure signal.

The statistical distribution the $p_{max}/p_{h,q}$-values is shown in Figure 9: this chart displays the relative percentages of: i) slightly breaking waves ($1<p_{max}/p_{h,q}<2.5$), ii) impact loads ($p_{max}/p_{h,q}\geq 2.5$) and iii) broken waves ($p_{max}/p_{h,q}\approx 1$) at each pressure transducer. These percentages were obtained by averaging the results of each single test. The chart shows a clear predominance (80-86%) of slightly breaking waves at each pressure transducer. A non-negligible number of wave loads is found at P2 and P3 (~8%), while the broken waves are more frequently observed at P1 (~17%).

More detailed analysis were performed to individuate further relationships between the breaker type and the structure geometry. In particular, the effects of: the wall height h_w, the berm width

B, the berm emergence h_b/H_s and the structure slope cot(α_d) were considered. The results of the analysis indicate that the impact loads ($p_{max}/p_{h,q}$≥2.5) tend to be slightly more frequent:

- in case of cot(α_d)=2, +4% on average (compare panel a to panel b of Figure 8);
- when the berm is at the swl (h_b=0), +3% on average (compare the continuous and dashed lines in Figure 8);
- in case of B=0.15 m, +4.5% on average (non-visible in Figure 8).

These effects result particularly modest and the variations (+3, +4, +4.5%) are comparable to the relative standard deviation $\sigma_{\%}$ (~4%) characterizing the distribution of the $p_{max}/p_{h,q}$-values. Therefore, it can be concluded that the majority of the wave impacts obtained with the new tests fall within the field of slightly-breaking waves, according to the PROVERBS classification and independently of the structure characteristics.

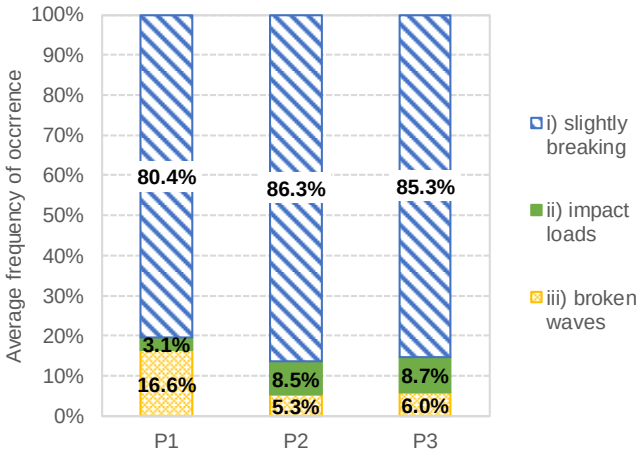

Figure 9. Average frequency of occurrence of the 3 breaker types found for the new tests at each pressure transducer along the wall. From left to right, from the wall basis to the wall top.

4.3. Parametric analysis of the wave pressures

This Sub-section proposes a parametric analysis of the effects of the main hydraulic and geometrical parameters on the wave pressures and their vertical distribution along the wall. For this purpose, the results are presented in terms of p_{250} as estimator of the extreme loads acting on the wall.

Both average and individual results relative to specific tests are introduced. The averages of the p_{250}-values calculated at each sensor P1, P2 and P3 are collected in Table 6. These average values have been firstly calculated by grouping the data into 2 datasets based on c2 and c4; then, for each dataset, the results are further divided based on: i) B=0.15 or 0.30 m; ii) presence or not of the parapet; iii) h_b/H_s=0 or 0.5. All the values have been made dimensionless through the group ($\rho g H_s$) according to other literature studies, a.o. Cuomo et al. (2010), Martinelli et al. (2018).

The same grouping criterion is proposed in Figure 10, which shows the vertical profiles of $p_{250}/(\rho g H_s)$ relative to 16 tests characterized by 16 different structure configurations under the same wave attack (H_s=0.06 m and $s_{m\text{-}10}$=0.03). In each panel of Figure 10, the 4 diagrams refer to the same slope (c2 or c4) and the same h_b/H_s, while they differ each other for B (0.15 and 0.30 m, represented with different shading but same line type) and for the absence or presence of the parapet (continuous ad dashed line, respectively). The 4 panels are meant to be compared to each other and present separately and in the order: the effect of the slope, from c4 (panels a and c) to c2 (panels b and d); the effect of h_b/H_s, which is increased from 0 (panels a and b) to 0.5 (panels c and d). The 16 profiles proposed in Figure 10 are example cases representative of all the other tests.

Table 6. Average values of $p_{250}/(\rho g H_s)$ at P1, P2 and P3. Averages computed on the datasets of tests at cot(α_d)=4 (upper part) and cot(α_d)=2 (lower part). In each part, data grouped by: B (3rd and 4th columns); structures with and without parapet (5th and 6th); values of h_b/H_s (7th and 8th).

	$p_{250}/(\rho g H_s)$ [-], μ-values; tests with cot(α_d)=4 (#64)						
Pressure transducer	All data with c4	Berm width		Inclusion of the parapet		Berm emergence	
		B=0.15	B=0.30	No	Yes	h_b/H_s=0	h_b/H_s=-0.5
P1	**1.56**	1.91	1.22	1.53	1.60	1.70	1.43
P2	**1.79**	2.19	1.38	1.80	1.78	2.18	1.40
P3	**1.20**	1.45	0.95	1.20	1.20	1.52	0.88
	$p_{250}/(\rho g H_s)$ [-], μ-values; tests with cot(α_d)=2 (#64)						
Pressure transducer	All data with c2	Berm width		Inclusion of the parapet		Berm emergence	
		B=0.15	B=0.30	no	Yes	h_b/H_s=0	h_b/H_s=-0.5
P1	**1.91**	2.01	1.76	1.79	2.00	2.03	1.78
P2	**2.37**	2.19	2.62	2.16	2.56	2.72	2.03
P3	**1.69**	1.49	1.95	1.47	1.87	1.95	1.43

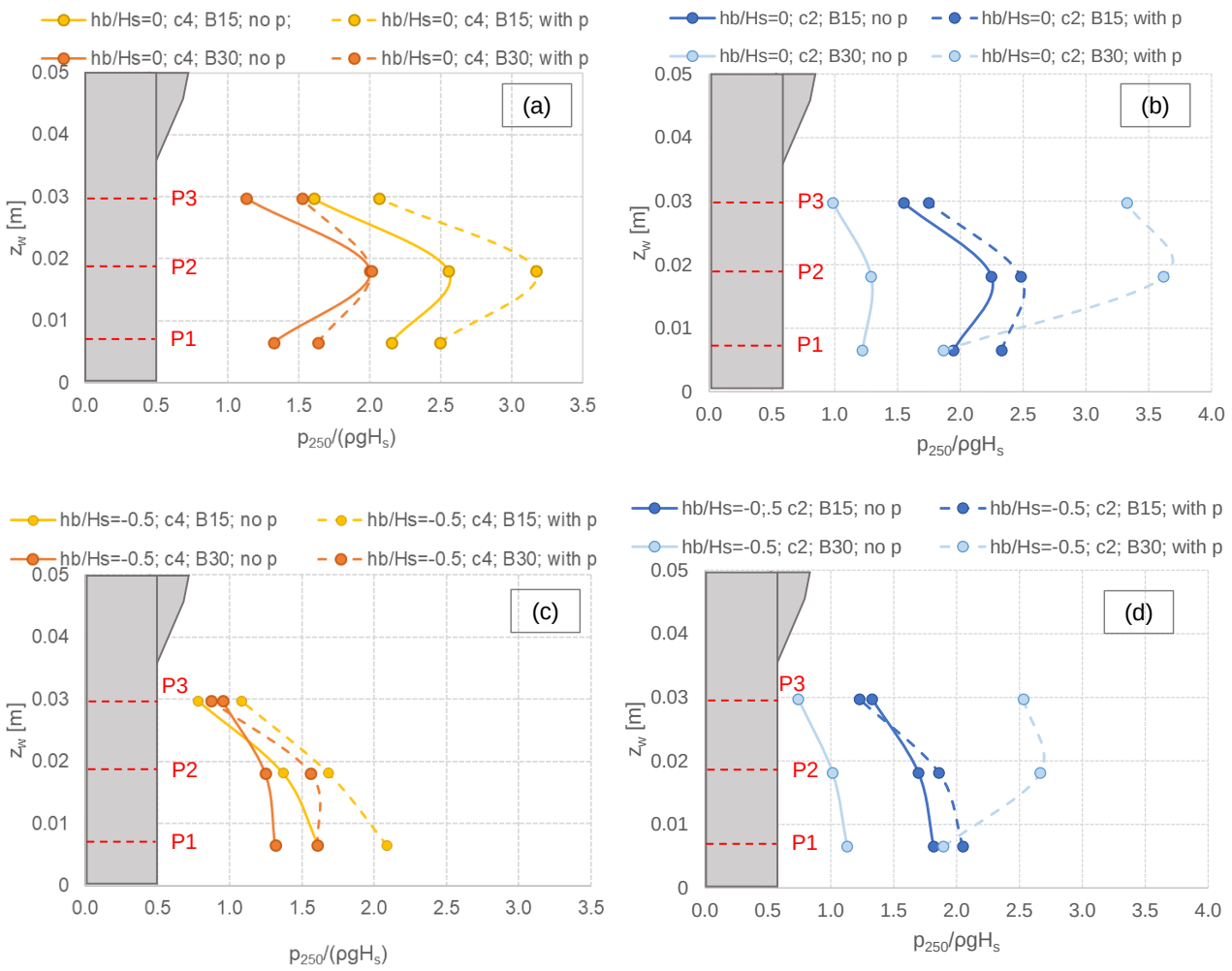

Figure 10. Vertical profiles of $p_{250}/\rho g H_s$ at P1, P2 and P3. Panels a,c: data at cot(α_d)=4; panels b, d: data at cot(α_d)=2; panels a, b: data at h_b/H_s=0; panels c, d: data at h_b/H_s=-0.5. In each panel: comparison between the same tests without and with parapet (continuous and dashed lines, respectively) and between the same tests with B=0.15 and 0.30 m (different shading).

With reference to Table 6 and Figure 10, the effect of each single parameter are analysed and discussed separately in the following Sub-sections 4.3.1, 4.3.2 and 4.3.3.

The effects of the wave steepness and of the wave height on the pressure values have been also investigated. Both these hydraulic parameters resulted to play pure “scale effects”, where the vertical profiles of p are simply translated towards lower and higher values for higher $s_{m-1,0}$ and H_s values, respectively. More specifically, the increase of $s_{m-1,0}$ from 0.03 to 0.04 determines an average reduction of the wave pressures of 12-15%, while the increase of H_s from 0.05 to 0.06 m determines an average increase of 10-12%. More details about this topic are given in Formentin et al. (2019a).

4.3.1. Berm emergence

The shape of the vertical distribution of the p-values is strongly dependent on the relative berm level, h_b/H_s (Figure 10 and Table 6).

When the berm is in correspondence of the swl (h_b/H_s=0, panels a and b of Figure 10), the pressure peak is always found at P2. This result is quantitatively confirmed by the average values of $p_{250}/(\rho g H_s)$ of Table 7, which are sensibly higher (≈+20-40%) at P2 ($p_{250}/(\rho g H_s)$=2.18 and 2.72 in case of c4 and c2, respectively) than at P1 (1.70 and 2.03) and at P3 (1.52 and1.95). When the berm is emerged (h_b/H_s=-0.5, panels c and d), the shape of the vertical distribution does not show the peak at P2 but presents a triangular distribution, with the maximum at P1 and the minimum in correspondence of P3. The different profiles are determined by the different run-up levels associated to the 2 berm conditions: at h_b/H_s=0, the run-up and the wave energy are higher and the overtopping tongue impinges against the crown wall approximately in correspondence of P2. At h_b/H_s=-0.5, the wave run-up is lower and the center of the overtopping tongue is localized around P1. This phenomenon is visually confirmed by the frames of the overtopping and impact events reproduced in Figure 11.

In terms of entity of the wave pressures, Figure 11 shows that for each test at h_b/H_s=-0.5 (panels c, d), the p_{250}-values are reduced of a minimum of 15% up to ~100% with respect to the same tests at h_b/H_s=0 (panels a, b). The entity of the reduction depends on the position of the pressure transducer (the higher the position, the higher the reduction) and on the structure configuration. Accordingly, the values of Table 6 indicate that the average reduction of p_{250} due to the berm emergence varies from 16% at P1 to 42% at P3 in case of c4 and from 12% at P1 to 27% at P3 in case of c2.

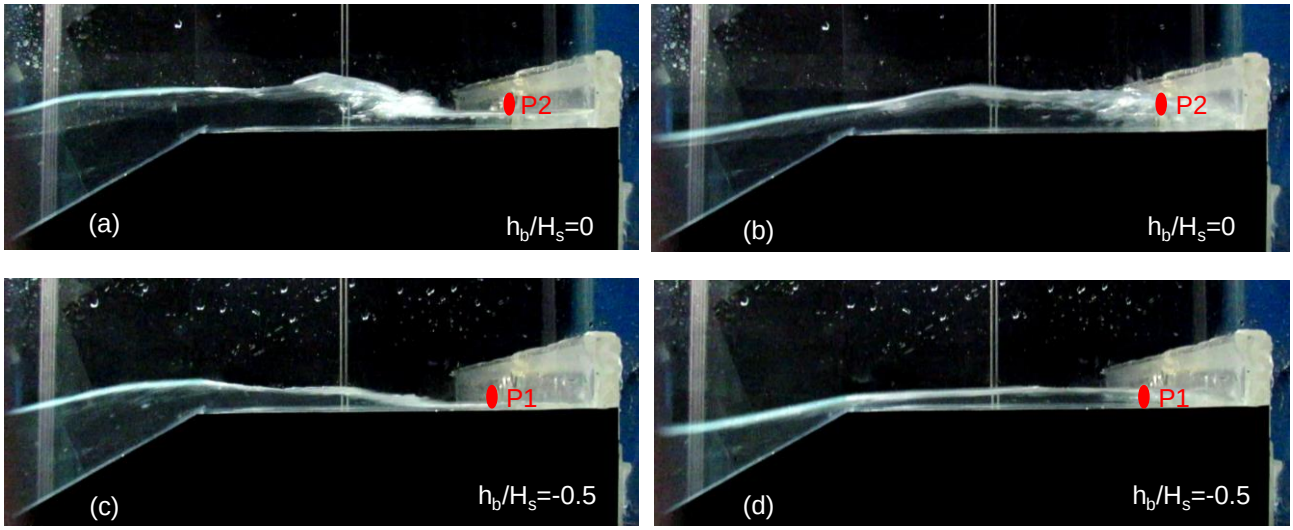

Figure 11. Consecutive frames of the same overtopping event (H_s=0.06 m, $s_{m-1,0}$=0.03) at the same structure (cot(α_d)=2, B=0.30 m, h_w=0.5 m, parapet) at h_b/H_s=0 (panels a and b) and h_b/H_s=-0.5 (panels c and d).

By combining the values of p_{250} with the number of impacts at the different transducers (Sub-section 4.1), it can be concluded that P1 and P2 are the sections of the crown wall subjected to the highest stresses in terms of both wave pressures and frequency of impact. More generally, the emergence of the berm (h_b/H_s) and the structure freeboard (R_c/H_s) are the principal parameters determining the entity, the frequency and the position of the impacts at the crown walls. This result is not trivial because it is valid for both breaking and non-breaking waves (structures c2 and c4), with and without parapet and independently of the berm width.

4.3.2. Berm width

Similarly to the overtopping discharge (Sub-section 3.2), the effect of *B* on the wave pressures is different for the 2 structure slopes. In case of c4, the increase of *B* from 0.15 to 0.30 m systematically reduces the *p*-values of ~35%, whereas no systematic effect is obtained with c2. The configuration with *B*=0.30 m in case of c2 even determines an increase of the pressures at P2 (~+20%) and P3 (~+30%), as it can be appreciated in all the charts of Figure 10 and from the values of Table 6.

In case of c4 ($\xi_{m-1,0}$<2), the highly turbulent overtopping flow along the berm caused by an early wave breaking (see Figure 4a) is characterized by a consistent amount of air entrainment and a huge energy dissipation rate: the wider *B*, the higher the dissipation and the lower the entity of the wave loads at the wall. The reduction obtained with *B*=0.30 m with respect to the same test at *B*=0.15 m is almost the same at the 3 pressure transducers, being on average ~35% and at maximum ~80%.

In case of c2, the non-breaking wave conditions determine higher run-up levels and thicker overtopping layers (compare Figure 4b to Figure 4a) and the thicker the water layer, the lower effect of the friction in the boundary layer along the berm surface and therefore the lower the wave energy dissipation. The result is a modest or negligible reduction of the wave impacts.

Overall, the reduction due to *B* is lower when the berm is emerged (~15%, compare Figure 10c to Figure 10a) and it tends to be more pronounced in presence of the parapet (dashed lines in each chart of Figure 10).

4.3.3. Parapet

The effects of the inclusion of the parapet are related to the structure slope and therefore to the wave breaking process.

Both Figure 10 (panels b and d) and Table 6 show that the parapet induces a systematic increase of the pressures along the whole vertical section of the crown wall in case of structures c2 (instead of c4). With respect to the same configuration and wave conditions, the increase of *p* due to the parapet in a structure c2 ranges between 10 and 70%, reaching and exceeding in

some cases the 100%. The increase rate increases with the wall height (on average, +10% at P1, +16% at P2 and +21% at P3) and it is maximum at P3.

The determination of higher impulsive pressures and forces along recurved seawalls, compared to vertical walls, is a well-known phenomenon (Kortenhaus et al., 2003; Castellino et al., 2018) related to the impulsive nature of the impact. When the waves impinge on the crown wall in non-broken conditions, the parapet blocks the overtopping flow of the surging waves, causing a sudden stop of the water mass horizontal momentum and generating a pressure shock wave (see Figure 4b). In the literature, the increase of the pressures at seawalls due to the presence of the parapet is sensibly higher (up to 2 times for breaking waves and even 10 times for surging non-breaking waves) with respect to the increase rates observed in the present study for structures c2 (up to 100%). This relatively modest increase is related to the different structure configurations – slopes with berm and crown wall instead of seawalls – which determine (~80%) wave impacts of the type “slightly-breaking” in most cases, and only marginally (~8%) wave impacts of the type “impact loads” (see Sub-section 4.2).

Different results are instead observed in case of breaking waves, i.e. for the slope c4. The average values of p_{250} for c4 in Table 6 show that there are no substantial differences when the parapet is included. Indeed, the same structure under the same wave attack was subjected to higher loads in some cases with the parapet and in other cases without the parapet. This result can be explained considering that the flow reaches the crown wall in fully-broken conditions (see Figure 4a), i.e. far from the impulsive nature of the non-breaking flow at seawalls and far from the slightly breaking conditions associated to the slopes c2.

5. Integrated analysis of the wave forces

The wave forces (F) obtained from the integration of the wave pressures along the crown walls are here presented and compared to the most recent literature formulae (Sub-sections 5.1 and 5.2). The first aim of the Section is to present the new data and asses their level of accuracy, with specific attention to potential scale and model effects. A refitting of a few of the existing formulae for the prediction of the extreme F_{250}-values is then proposed to improve the representation of the structure slope effects. Finally, this Section proposes a new, simple fitting to link the average overtopping discharge q to the extreme forces F_{250} at walls, based on the approach by Molines et al. (2018) (Sub-section 5.3).

5.1. Literature overview

Although several studies on the analysis of wave impacts at crown walls on top of rubble mound breakwaters are available (a.o., the most recent works are: Franco et al., 2018; Jacobsen et al., 2018; Van Gent and Van der Werf, 2019; Mares-Nasarre and Van Gent, 2020), the literature specifically dedicated to storm walls on top of smooth dikes is very limited.

Chen et al. (2015) investigated a similar geometry, carrying out 118 2D-physical model tests of wave impacts at storm walls on a dike berm with a shallow foreshore (B=0.25-0.75 m; cotα_d=3 and 6; h_b=-0.012 and -0.052 m; h_w=0.50 m; other parameters characterizing the dataset are collected in Table 7). These experiments were conducted at the Flanders Hydraulic Research (Antwerp, Belgium) and they all consisted of regular waves, of which 79 repeated tests. The study prompted the following formula to predict the total overtopping flow load F_t, based on the overtopping momentum flux:

$$\frac{F_t}{\rho g (d_{A0})^2} = 1.7 \cdot C_{tr}^2 \cdot \cot\alpha_d \cdot \exp\left(-3.08 \cdot \cot\alpha_d \cdot \frac{B}{L}\right), \quad \begin{cases} C_{tr} = 0.33 \cdot \ln\left(\frac{B}{L}\right) + 1.86 \\ d_{A0} = 0.77 \cdot H \cdot (1 - \frac{R_c}{R_u}) \end{cases}, \tag{8}$$

where: d_{A0} is the unobstructed overtopping flow depth over the dike berm, C_{tr} is an empirical coefficient to correlate d_{A0} to the obstructed flow depth, R_u is the wave run-up and H and L are, respectively, the wave height and the wave length of the regular waves. The same structures tested by Chen et al. (2015) were later subjected to a new set of irregular wave conditions, to investigate the statistical distribution of the overtopping forces on the vertical wall and derive a procedure to determine the expected maximum overtopping force for a specific design condition (Chen et al., 2016). Van Doorslaer et al. (2017), proposed the first design formula for predicting the wave forces on a smooth dike crown wall under irregular, non-breaking waves:

$$\frac{F_{250}}{\rho g R_c^2} = a_F \cdot \exp\left(b_F \cdot \frac{R_c}{H_{m0}}\right), \tag{9}$$

Eq. (9) considers the dimensionless quantity $F_{250}/\rho g R_c^2$, where ρ is water density, and predicts an exponential decreasing trend of the wave forces with the relative freeboard R_c/H_{m0}
Eq. (9) was developed based on 3 different sets of experiments on dikes with sloping promenades and crown walls without parapet carried out at different scales, from 1:10 to 1:15. These experiments were performed in different laboratory facilities: the wave flume at Ghent University, UGent hereinafter, the GWK in Hannover, GWK hereinafter, and the CIEM wave flume of the Universitat Polytecnica de Barcelona, UPC hereinafter. The values of the fitting coefficients a_F and b_F of Eq. (9), which vary upon the model scale and the cross-section geometry, are reported in Table 7. The main parameters characterizing these datasets are presented in Table 8.

Recently, De Finis et al. (2020) proposed a refitting of Eq. (9) based on new numerical tests carried out at the Università Roma 3 (UR3 dataset, hereinafter) extending the UPC dataset with various promenade lengths and wall heights and breaking waves, see Table 8. The new formula, which represents a refined version of Eq. (9) including the parameters $\xi_{m-1,0}$, B and h_w, reads as follows:

$$\frac{F_{250}}{\rho g R_c G_c} = a \cdot \exp\left(-b \cdot \frac{R_c}{H_{m0} \cdot \xi_{m-1,0}}\right)^{\alpha} \cdot \left(\frac{B}{h_w}\right)^{\beta}, \text{ with } a=0.947,\ b=1.407,\ \alpha=0.753,\ \beta=0.468. \tag{10}$$

where the values of the coefficients α, β, a and b are optimized to fit the datasets UPC and UGent and the new numerical data by De Finis et al. (2020).

Only the formulae proposed by Van Doorslaer et al. (2017) and De Finis et al. (2020) are suitable for comparison with the new experiments at Unibo, due to the tests performed under irregular waves, due to the cross section similarities and due to the similar range of the hydraulic and structural parameters. However, the new tests include specificities, such as the berm at the swl and the presence of the sloping parapet (covering together the 75% of the database), which have never been investigated before (in terms of wave forces) and which are therefore out of the range of validity of all the mentioned formulae.

Table 7. Values of the coefficients a_F and b_F of Eq. (9) and in Figure 12.

Scale	Laboratory	Geometry	a_F	b_F	Eq.	Ref. in Fig. 12	R^2 (formula - Unibo data)
1:10-1:15	UGent	Promenade and wall	7.80	-2.02	(9)	a	0.74
1:6	UPC	Promenade and wall	7.80	-2.40	(9)	b	0.74
1:10-1.15	UGent	Promenade, wall and parapet	8.60	-1.67	(9)	c	0.75

Table 8. Range of the main hydraulic and structural parameters characterizing the tests at Unibo grouped by cot(α_d) and the datasets by Van Doorslaer et al. (2017) and by De Finis et al. (2020).

				Datasets used by De Finis et al. (2020)		
Experiments at Unibo (scale 1:20)			Datasets by Chen et al. (2015) (regular waves)	Datasets used by Van Doorslaer et al. (2017)		UR3 (numerical data, 1:1)
				UGent (scale 1:10-1:15)	UPC (scale 1:6)	
cot(α_d)	2	4	3; 6	2; 3	3	3
h_b/H_{m0}	-0.75 – +0.12	-1.13 – +0.09	-1.30; -0.16	-1.22 – -0.23	-1.23 – 0	-0.97 – 0
R_c/H_{m0}	0.66 –2.20	0.69 – 2.51	6.74; 13.8	0.91 – 2.07	0.54 – 2.10	0.36 – 2.51
$B/L_{m-1,0}$	0.07– 0.27	0.07 – 0.26	0.01 – 0.21	0.13 – 0.25	0.08 – 0.16	0.02 – 0.95
h_w/R_c	0.86 – 1.82	0.52 – 1.09	0.91-0.98	0.36 – 0.67	0.36 – 0.87	0.22 – 0.94
$s_{m-1,0}$	0.015 – 0.048	0.017 – 0.041	0.003-0.021	0.010 – 0.036	0.013 – 0.033	0.014 – 0.073
$\xi_{m-1,0}$	2.28 – 4.03	1.23 – 1.94	2.3-10	2.24 – 4.79	1.83 – 2.84	1.23 – 2.80

5.2. Comparison with existing formulae

In the present Sub-section, the values of the wave forces F_{250} obtained from the integration of the pressure data are compared with the predicting formulae (9) and (10) presented in Sub-section 5.1.

Figures 12 and 13 show respectively the comparison of the new tests with Eq. (9) and (10). In each Figure, the new data are separated by cot(α_d) (c2 and c4 in panels a and b, respectively), by B (B15 and B30, circles and diamonds, respectively) and based on the presence or not of the parapet (void and filled-in symbols, respectively). The available literature data used to derive the two formulae are also represented by shaded areas. Only the UR3 numerical data include breaking conditions and can be therefore used for comparison in Figure 13, panel b.

The sensitivity of the new data to the presence of the parapet is in line with the findings relative to the wave pressures (see Sub-section 4.3.3). Most of the tests at c2 with parapet (panels a of Figures 12 and 13, void symbols) show slightly higher F_{250}-values than the same tests without parapet (filled-in symbols). This effect is not evident for the tests at c4 (panels b of Figures 12 and 13), which do not show any particular trend with the parapet.

The new data under non-breaking conditions (Figures 12a, 13a) show a good agreement with the available literature data, even if the scale is smaller than the UGent and UPC scale (Table 8). In case of breaking conditions instead (Figure 13b), it can be appreciated that there is a significant shift (30%) among the UR3 numerical data and the new experiments. This discrepancy can be explained not only by the different scale that may affect the breaking and air entrainment processes but also by the different slopes in the two datasets (c3 and c4 respectively for the UR3 data and for the new tests). Therefore the overestimation of the new measured forces with respect to the UR3 dataset cannot be used indirectly as a measure to quantify the scale and model effects (Section 2.3).

The R^2-values among the Unibo data and the different fittings by Eq. (9) are reported in the last column of Table 8. Eq. (9) with a_F=7.80, b_F=-2.02 (case ‘a’ and dashed line in Figure 12a) leads to an overall good agreement among data and formulae, with slight overestimation of the F_{250}-values in case of c4 (panel b), which might be explained with the smaller scale adopted (1:20), and, specifically, with a potential increase of the surface tension and a reduced amount of air entrainment. On the contrary, the use of a_F=7.80, b_F=-2.40 (case ‘b’, continuous line) would lead to a systematic underestimation of the new data, while the use of a_F=8.60, b_F=-1.67 (case ‘c’, dot-dashed line), corresponding to the fitting for the Ugent tests with parapet, would represent an upper envelope to the Unibo data. Therefore, the average-cautious representation obtained with a_F=7.80, b_F=-2.02 is preferred. The different representation of the 2 datasets c2 and c4 can be justified considering that Eq. (9) was fitted on data characterized by slopes cot(α_d)=2 and 3 (see Table 8), i.e. exclusively on non-breaking waves.

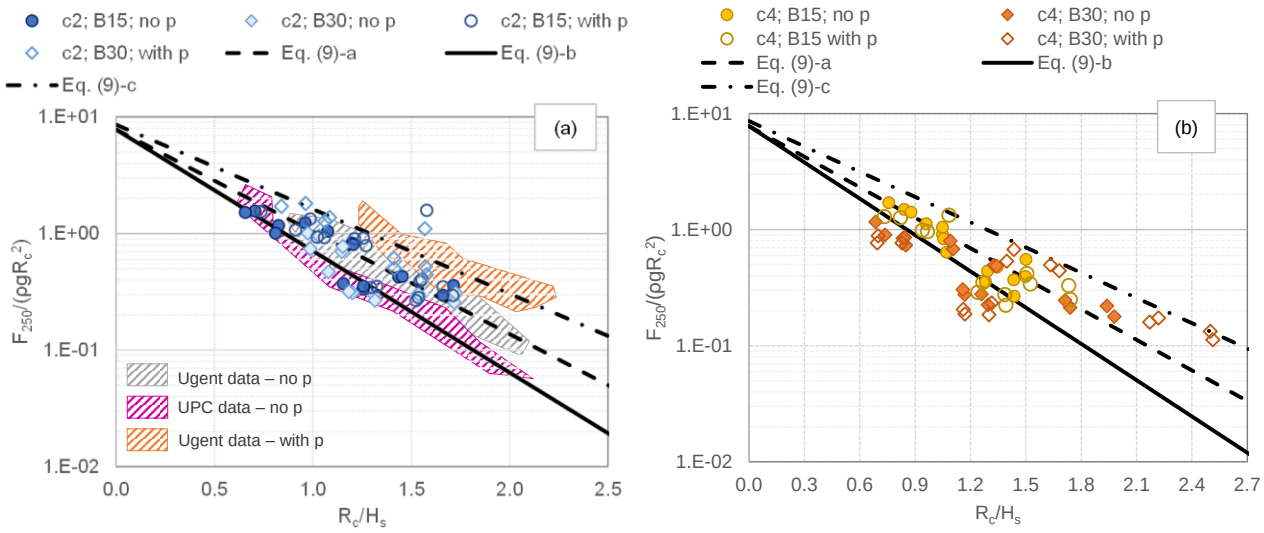

Figure 12. Dimensionless F_{250}-values from the new experiments at Unibo compared to the lines representing Eq. (9). Tests with c2 (panel a) and c4 (panel b) grouped by values of B and by the inclusion or not of the parapet. The shaded areas (in panel a) identify the data available from the literature and used in the works by Van Doorslaer et al. (2017) and Van Doorslaer (2018) for the development of Eq. (9).

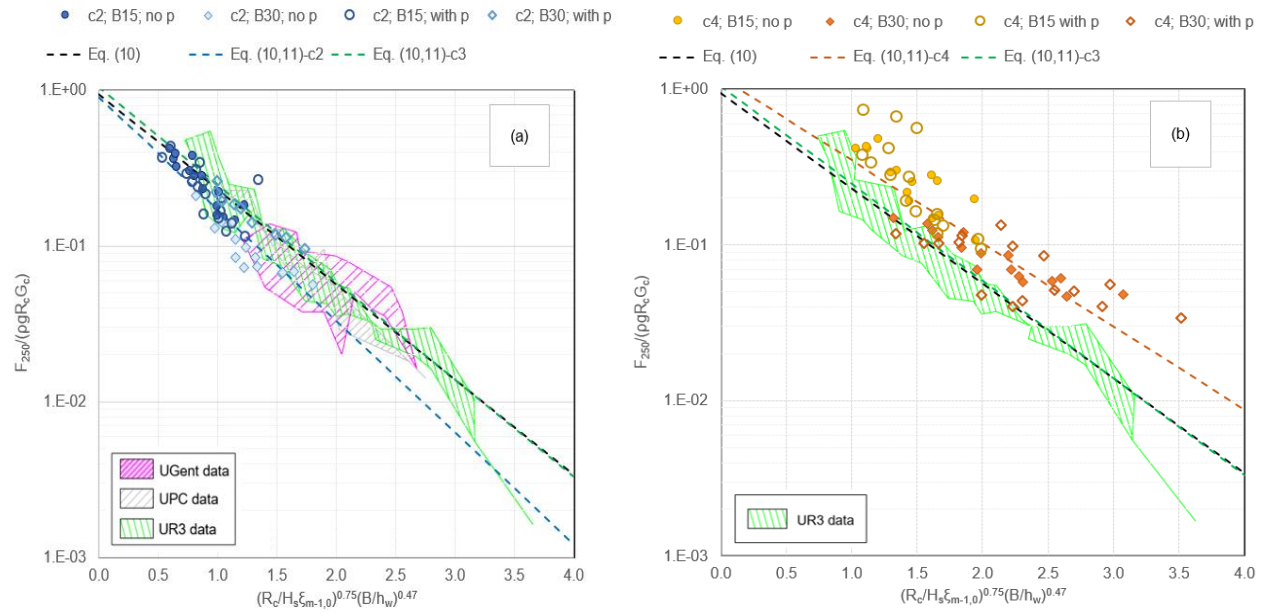

Figure 13. Dimensionless F_{250}-values from the new experiments at Unibo compared to the lines representing Eqs. (10) and (10,11). Tests with c2 (panel a) and c4 (panel b) grouped by values of B and by the inclusion or not of the parapet. The shaded areas identify the data available from the literature and used in the work by De Finis et al. (2020) for the development of Eq. (10).

Figure 13 compares the new data with Eq. (10) that accounts for the effects induced by the slope angle and by the wave breaking through the parameter $\xi_{m-1,0}$. The new data of F_{250} are indeed systematically overestimated or underestimated by Eq. (10) in case c2 or c4, respectively. The

best fitting can be obtained by introducing the following modifications to the coefficients *a* and *b* of the formula by De Finis et al. (2020):

$$\begin{cases} a=0.15\cdot\cot(\alpha_d)+0.60 \\ b=0.21\cot(\alpha_d)-2.07 \end{cases}. \quad (11)$$

Note that when $\cot(\alpha_d)=3$, Eq. (11) gives $a=1.05$ and $b=1.44$, i.e. values very close to the original ones. The fitting representing Eq. (10) with the new coefficients *a* and *b* provided by Eq. (11) are shown in Figure 13a,b as dashed lines. The values of the determination coefficient characterizing the agreement among the formula and the new data are respectively $R^2=0.89$ and $R^2=0.79$ for c2 (panel a) and c4 (panel b). The application of Eq. (10) to the numerical data by De Finis et al. (2020) and to the UPC dataset with the original and with the new coefficients by Eq. (11) (Figures 13a, b) give almost the same results, with $R^2=0.84$ in both cases.

In conclusion, the new data on F_{250} verify and extend the validity of Eq. (9) to the ranges of the parameters reported in Table 8 and to the smaller scale of 1:20. The same results apply also to Eq. (10) if including the correction proposed with Eq. (11). The new fitting Eq. (11) should be verified, especially in case of breaking waves, at larger scale and under storm conditions before using for design purpose.

5.3. A new fitting for predicting the wave forces from the wave overtopping discharge

The objective of this Sub-section is to verify the dependence of F_{250} on q for smooth dike-berms by means of a simple mathematical relation, following the approach by Molines et al. (2018). Such relation is strictly dependent on the structure geometry. Since there are already tools allowing to predict q for a variety of structural configurations under a variety of wave conditions (a.o., the recent tool based on the gradient-descent algorithm by Den Bieman et al., 2020 or the neural networks by Van Gent et al. (2007) and by Zanuttigh et al. (2016) and Formentin et al. (2017), such simple relation would allow the direct prediction of F_{250} as well.

Wave overtopping discharges and wave loads are the result of the same physical processes, i.e. wave breaking, run-up and overtopping. For slightly breaking waves, as most of the waves in front of the crown wall in these experiments (80-85%, see Sub-section 4.2 and Figure 9), the pressure signals at the walls show peaks (F_{max}) which are higher than the following quasi-static peaks ($F_{h,q}$), but the ratio values $F_{max}/F_{h,q}$ are relatively modest (<2.5) and no real impulsive conditions occur ($F_{max}/F_{h,q}$>2.5). In such conditions, the waves go up and down the wall without producing extreme pressure and force peaks, the formation of air pockets below the plunging wave crest is limited and no water jets rushing vertically upwards are observed. Therefore, the greater the run-up, the greater the overtopping at the structure crest and the greater the overtopping inshore the crown wall and the greater the force on the wall itself.

The new data show the following linear dependence of F_{250} on q:

$$\frac{F_{250}}{\rho g R_c^2} = 2000 \cdot \frac{q}{g H_s T_{m-1,0}} + 0.3 \qquad (12)$$

where the empirical coefficients of Eq. (12) are optimized to fit these new tests. Since the test duration is limited to 500 waves, Eq. (12) may give a cautious estimate of F_{250}..

The linear relationship is the result of the use of the dimensionless quantities $F_{250}/\rho g R_c^2$ *and* $q/gH_sT_{m-1,0}$, which include intrinsically the exponential dependences with R_c/H_s and $\xi_{m-1,0}$ (see Eq.s (1) and (9) for q and F_{250}, respectively). The presence of the 0-degree term (0.3) in Eq. (12) suggests that F_{250} is not equal to 0 even when q=0. This is due to the fact that q is calculated *behind* the wall, while F_{250} is calculated *at* the wall. Therefore, the 0-degree term represents – for these tests – the dimensionless entity of the wave impact consequent to an overtopping event that hits and stops against the wall.

The Unibo experimental data are compared to Eq. (12) in Figure 14, where are grouped by values of cot(α_d) and by the inclusion or not of the parapet. The level of agreement among the data and the formula is quantified in terms of relative standard deviation $\sigma_{\%}$ and R^2-values in Table 9 for the whole database ($\sigma_{\%}$=0.37, R^2=0.81) and the single datasets. Both Figure 14 and Table 9 indicate that the data are similarly well represented both in presence of parapet ($\sigma_{\%}$=0.37, R^2=0.80) and not ($\sigma_{\%}$=0.37, R^2=0.82), while the dataset c2, relative to non-breaking wave conditions, is slightly more scattered (σ=0.39, R^2=0.78) than the dataset c4 ($\sigma_{\%}$=0.33, R^2=0.86). Indeed the tests at c2 present an intrinsic higher variability of the q and F_{250}-values, since they are, on average, characterized by higher overtopping rates and higher impact loads. In other terms, the higher scatter associated to the dataset c2 does not indicate a worse agreement with the formula, but it reflects the wider distribution of the q and F_{250}-values themselves. Nevertheless, a modest effect of the slope seems evident in Figure 14, as the c2-data are, on average, collocated slightly below the c4-data. However, the inclusion of the representation of the slope angle in Eq. (12) would require with the systematic test of different cot(α_d)-values.

Note that Eq. (12) is not meant to replace consolidated and more classical formulae specifically conceived to derive F_{250} from the "traditional" parameters (see, e.g., Sub-section 5.1). However, it may provide a first, rough estimate of F_{250} of practical utility in case of existing experiments focused on the measurement of the wave overtopping discharge, where only the q-data are available. The relation holds only in case of structures with the same geometry and within the limits of the tested hydraulic conditions.

Table 9. Error indices σ and R^2 characterizing the agreement between the data of F_{250} and corresponding predictions from Eq. (12).

	All data	**cot(α_d)**		**parapet**	
		c4 (breaking)	c2 (non-breaking)	No	yes
$\sigma_{\%}$	0.37	0.33	0.39	0.37	0.37
R^2	0.81	0.86	0.78	0.82	0.80

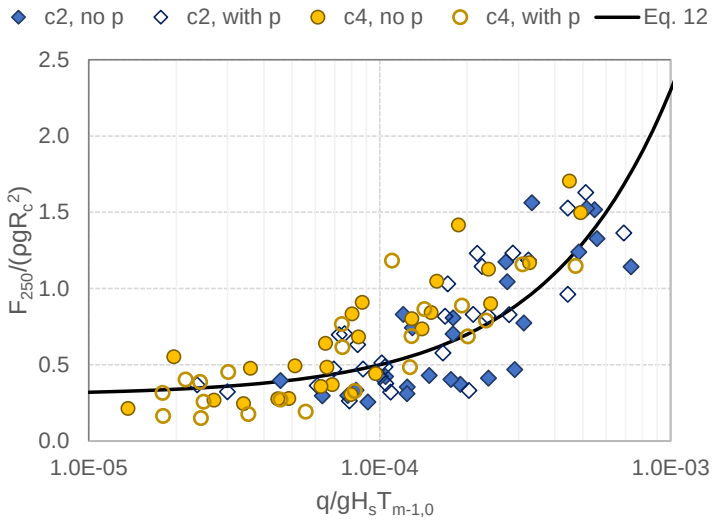

Figure 14. Dimensionless F_{250} and q-values resulting from the experiments at Unibo compared to the new formula by Eq. (12).

6. Conclusions

This contribution presented 128 new small scale experiments on wave overtopping at smooth berms with crown walls under irregular waves carried out in the wave flume of the Hydraulic Laboratory at the University of Bologna.

Based on these new experimental results, a parametric analysis of the effects of upgrading a smooth berm with i) the widening of the berm width B, ii) the extension of the wall height h_w; iii) the inclusion of a sloping parapet; has been performed and the following indications can be drawn by keeping constant all the other structural and hydraulic parameters.

The reduction of q can be achieved by small increase of h_w, whose extension of +25% with respect to the benchmark case leads to a reduction of q of ≈50%, for most of the tested conditions. In case of breaking waves, the reduction of q of ≈35% can be obtained with the geometrical upgrade of B of +100%. In case of medium-low values of q, the introduction of the parapet produces the increase of the reduction rate of q from 0% to 70% with q decreasing from 10^{-3} to ~10^{-5} $m^3/(sm)$.

The parameters berm submergence h_b/H_s and the wall crest freeboard R_c/H_s affect most significantly the entity, the frequency and the position of the impacts at the crown walls for both breaking and non-breaking waves, with and without parapet and independently of B. In case of non-breaking waves, the inclusion of the parapet induces a severe increase (up to 100%) of the p_{250}–values along the whole vertical section of the crown wall. In case of breaking/broken waves, the increase of B reduces the enhanced loads (up to 60%) due to the introduction of the parapet.

New formulations are proposed to predict the average and the maximum values of the frequency of the wave impacts (*Nimp/Now*) at different locations along the wall height, (Eq. 7), and to fit

the coefficients of the formula by De Finis et al. (2020) for the prediction of the F_{250}-values at the crown walls, (Eq. 10).
A new linear relationship between the 2 dimensionless quantities $F_{250}/\rho g R_c^2$ and $q/gH_sT_{m-1,0}$ is proposed, Eq. (11), that might be used to eventually derive the F_{250}-values based on measured or predicted values of q. This relation holds only in case of slightly breaking (plunging and surging) waves at the wall ($F_{max}/F_{h,q}$<2.5) and within the range of the tested structural and hydraulic parameters.

All these (qualitative and quantitative) indications and new fittings (Eq.10, 11) are valid for smooth structures, characterised by the same geometry and under wave attacks within the tested hydraulic conditions. Experiments at larger scale and under severe storms are recommended to verify and extend the present results for design purpose.

List of notations

a	Empirical coefficient of Eq.s (10) and (11)
b	Empirical coefficient of Eq.s (10) and (11)
a_F	Empirical coefficient of Eq. (9)
b_F	Empirical coefficient of Eq. (9)
ANN	Acronym of Artificial Neural Network
B	Berm width
B_{eq}	Equivalent berm width in case of structure with parapet (for ANN)
c2, c4	Abbreviations of cot(α_d)=2, cot(α_d)=4
C_{tr}	Empirical coefficient of Eq. (8)
d_{A0}	Unobstructed overtopping flow depth over the dike berm, defined as in Eq. (8)
Eff	Hydraulic effectiveness of a structural upgrade, defined as in Eq. (3)
F	Instantaneous wave force obtained from the integration of the wave pressures
F_{max}	maximum wave force
F_{mean}	time average of the wave forces distribution
F_{median}	time median of the wave forces distribution
F_n	n-th quantile of the wave forces distribution, with n=100, 250

F_t	Total wave force in case of regular waves (Eq. 8)
g	Acceleration due to gravity
h	Water depth or thickness or level
h_b	Berm submergence (h_b<0 and h_b>0 respectively for emerged and submerged berm)
h_c	Elevation of the structure berm with respect to the bottom of the channel, excluding the crown wall
h_n	Parapet height
h_w	Height of the crown wall
H	Wave height referring to regular waves
H_{m0}	Spectral wave height
H_s	Significant wave height at the toe of the structure
L	Wave length referring to regular waves
$L_{m-1,0}$	Wave length from spectral analysis
N	Number of waves
Now	Number of overtopping waves
Nimp	Number of wave impacts at the wall
Nimp_d	Distribution of the number of the wave impacts along the wall
p	Instantaneous wave pressures
p_{hq}	quasi-hydrostatic pressure
p_{max}	maximum wave pressure
p_{mean}	time average of the wave pressures distribution
p_{median}	time median of the wave pressures distribution
$p_{min\ threshold}$	minimum vertical drop in the *p*-signal to identify an “actual” impact event (instead than a small oscillation or noise (calibration parameter of the *Matlab* procedure to identify the impact event)
p_n	n-th quantile of the wave pressures distribution, with n=100, 250
P_i	Position of the i-th pressure transducer installed along the crown wall

q	Average specific wave overtopping discharge
q^*	Dimensionless average specific wave overtopping discharge, $q^*=q/(gH_{m0}T_{m-1,0})$
q_{basic}	Value of q corresponding to a dike configuration without structural upgrades
$q_{upgraded}$	Value of q corresponding to a dike configuration including one or more structural upgrades
swl	Acronym of “still water level”
R^2	Coefficient of determination
R_c	Structure freeboard with the respect to the still water level ($R_c=h_w-h_b$)
$R_{c,eq}$	Equivalent freeboard in case of structure with parapet (for ANN)
R_u	Wave run-up
rmse	Root Mean Squared Error
$s_{m-1,0}$	Wave steepness calculated based on the spectral wave period
$t_{min\ delay}$	minimum time-delay that is expected to occur between two consecutive peaks in the pressure signal (calibration parameter of the *Matlab* procedure to identify the impact event)
$T_{m-1,0}$	Spectral wave period
UGent	Abbreviation referring to the tests performed at the Ghent University
UPC	Abbreviation referring to the tests performed at the Universitat Polytecnica de Barcelona
UR3	Abbreviation referring to the tests performed at Università Roma 3
wgs	Acronym of “wave gauges”
z_w	Ordinate elevation along the crown wall ($z_w=0$ and $z_w=h_w$ respectively at the basis and at the top of the wall)
α_d	Dike off-shore slope below the berm
γ^*_{GP}	Reduction factor of q accounting for the presence of a berm, crown wall and parapet
ε	Angle of inclination of the parapet
λ	Ratio between the wall height h_w and the parapet height h_n
μ	Mean
$\xi_{m-1,0}$	Iribarren-Battjes breaker parameter

σ	Standard deviation
$\sigma_{\%}$	Relative standard deviation (or coefficient of variation)

Acknowledgments

The support of the European Commission through the Horizon 2020 project BRIGAID ("BRIdging the GAp for Innovations in Disaster resilience," www.brigaid.eu) is gratefully acknowledged.

References

Altomare, C., Gironella, X., 2014. An experimental study on scale effects in wave reflection of low-reflective quay walls with internal rubble mound for regular and random waves, Coastal Engineering, 90, 51-63.

Bullock G.N., Obhrai C., Peregrine D.H. and Bredmose, H., 2007. Violent breaking wave impacts. Part 1: Results from large-scale regular wave tests on vertical and sloping walls, Coastal Engineering, 54, 602-617.

Burcharth, H.F., Lykke Andersen, T. and Lara, J.L., 2018. Upgrade of coastal defence structures against increased loadings caused by climate change: a first methodological approach. Coastal Engineering 87, 112–121.

Castellino M., Sammarco P., Romano A., Martinelli L., Ruol P., Franco L. and De Girolamo, P. 2018. Large impulsive forces on recurved parapets under non-breaking waves. A numerical study. Coastal Engineering 136, 1-15.

Chen X., Hofland B., Altomare C., Suzuki T., Uijttewaal W., 2015. Forces on a vertical wall on a dike crest due to overtopping flow, Coastal Engineering 95, 94–104.

Chen X., Hofland B., Uijttewaal W., 2016, Maximum overtopping forces on a dike-mounted wall with a shallow foreshore, Coastal Engineering116, 89–102.

Chen X., Hofland B., Molenaar W., Capel A., Van Gent M.R.A., 2019. Use of impulses to determine the reaction force of a hydraulic structure with an overhang due to wave impact, Coastal Engineering 147, 75–88.

Cooker, M.J., Peregrine, D. H., 1995. Pressure -impulse theory for liquid impact problems, Journal of Fluid Mechanics, Cambridge University Press, 297, 193-214.

Cuomo G., Allsop W., Bruce T. and Pearson, J., 2010. Breaking wave loads at vertical seawalls and breakwaters, Coastal Engineering 57, 424-439.

De Finis S., Romano A. and Bellotti G., 2020. Numerical and laboratory analysis of post-overtopping wave impacts on a storm wall for a dike-promenade structure, Coastal Engineering 155, 103598, 13 pp.

Den Bieman J.P., Wilms J.M., Van den Boogaard H.F.P., Van Gent M.R.A., 2020, Prediction of Mean Wave Overtopping Discharge Using Gradient Boosting Decision Trees, Water 12, 1703.

EurOtop, 2018. Manual on wave overtopping of sea defences and related Structures. An overtopping manual largely based on European research, but for worldwide application. N.W.H. Allsop, T. Bruce, J. DeRouck, A. Kortenhaus, T. Pullen, H. Schüttrumpf, P. Troch, J.W. van der Meer and B. Zanuttigh. www.overtopping-manual.com

Formentin S.M., Zanuttigh B. and J.W. van der Meer. 2017. A neural network for predicting wave reflection, overtopping and transmission, Coastal Engineering Journal, 59, No. 2, 1750006, 31 pp.

Formentin S.M. and Zanuttigh B., 2018. A new method to estimate the overtopping and overflow discharge at over-washed and breached dikes, Coastal Engineering 140, 240-256.

Formentin S.M. and Zanuttigh B., 2019. A Genetic Programming based formula for wave overtopping by crown walls and bullnoses, Coastal Engineering 152, 103529, 17 pp.

Formentin S.M., Zanuttigh B., Palma G, Gaeta M.G. and Guerrero M., 2019a. Experimental analysis of the wave loads on dike crown walls with parapets, Proc. of Coastal Structure Conference, Hannover (D), 2019.

Formentin S.M., Gaeta M.G., Palma G., Zanuttigh B. and Guerrero M., 2019b. Flow depths and velocities across a smooth dike crest, Water 11(10), 2197.

Franco, L., Geeraerts, J., Briganti, R., Willems, M., Bellotti, G. De Rouck, J., 2009. Prototype measurements and small-scale model tests of wave overtopping at shallow rubble mound breakwaters: the Ostia-Rome yacht harbour case. Coastal Engineering 56, 154-165.

Franco, L., Belotti, G. and Cecioni, C., 2018. Physical model tests of wave overtopping and forces on breakwater crown walls, in Proceedings of 36th ICCE, Baltimore (MD), 2018.

Galvin C.J., 1964. Wave-height prediction for wave generators in shallow water. Washington (DC): U.S. Army Corps of Engineers. Technical Memorandum No. 4, 1-20.

Hofland B., Kaminski M.L., Wolters G., 2010. Large scale wave impacts on a vertical wall, Proc. of 32nd ICCE, Shanghai (China), 2010.

Hughes, S. A., and Nadal, N. C., 2009. Laboratory study of combined wave overtopping and storm surge overflow of a levee, Coastal Engineering, 56(3), 244-259.

Jacobsen, N.G., Van Gent, M.R.A., Capel, A., Borsboom, M., 2018. Numerical prediction of integrated wave loads on crest walls on top of rubble mound structures, Coastal Engineering 142, 110-124.

Jonkman, S.N., Hillen M., Nicholls R. J., van Ledden M. 2013. Costs of Adapting Coastal Defences to Sea-Level Rise— New Estimates and Their Implications. Journal of Coastal Research, 290(5), 1212-1226.

Kisacik, D., Troch, P. and P. Van Bogaert, 2012. Description of loading conditions due to violent wave impacts on a vertical structure with an overhanging horizontal cantilever slab, Coastal Engineering, 60, 201-226.

Kortenhaus A., Pearson, J. Bruce, T. Allsop W., Van der Meer J., 2003. Influence of parapets and recurves on wave overtopping and wave loading of complex vertical walls. Proc. Coast. Struct. 2003, 369–381.

Kudale M.D., Bharelao A.R., 2015. Equivalent monochromatic wave height for the design of coastal rubble mound structures, Aquatic Procedia 4, 264 – 273.

Lykke Andersen, T., Burcharth, H.F. and Gironella, X., 2011. Comparison of new large and small scale overtopping tests for rubble mound breakwaters, Coastal Engineering 58, 351-373.

Martinelli L., Ruol P., Volpato M., Favaretto C., Castellino M., De Girolamo P., Franco L., Romano A. and Sammarco P., 2018. Experimental investigation on non-breaking wave forces and overtopping at the recurved parapets of vertical breakwaters, Coastal Engineering 141, 52-67.

Mares-Nasarre P. and Van Gent M.R.A., 2020. Oblique Wave Attack on Rubble Mound Breakwater Crest Walls of Finite Length, Water 12, 353

Martin, F.L., Losada, M.A., Medina, R., 1999. Wave loads on rubble mound breakwater crown walls. Coastal Engineering 37 (2), 149–174.

Molines J., Herrera M.P. and Medina J.R., 2018. Estimations of wave forces on crown walls based on wave overtopping rates, Coastal Engineering 132, 50-62.

Nicholls, R.J., 2002. Analysis of global impacts of sea-level rise: a case study of flooding, Phys. Chem. Earth, 27(32), 1455-1466.

Nørgaard, J.Q.H., Andersen, T.L., Burcharth, H.F., 2013. Wave loads on rubble mound breakwater crown walls in deep and shallow water wave conditions, Coastal Engineering 80, 137–147.

Oumeraci H., Klammer, P., and Partenscky H.W. 1993. Classification of breaking wave loads on vertical structures' Journal of Waterway, Port, Coastal and Ocean Engineering, 119(4), 381-397.

Palma, G., Contestabile, P., Zanuttigh, B., Formentin, S.M., Vicinanza, D. 2020. Integrated assessment of the hydraulic and structural performance of the OBREC device in the Gulf of Naples, Italy. Applied Ocean Research, 101, 102217.

Pedersen, J., 1996. Wave Forces and Overtopping on Crown Walls of Rubble Mound Breakwaters. Series paper 12. Hydraulic and Coastal Engineering Laboratory, Department of Civil Engineering, Aalborg University, Denmark.

Ravindar R, Sriram, V., Schimmels S. and D. Stagonas 2019, Characterization of breaking wave impact on vertical wall with recurve, ISH Journal of Hydraulic Engineering, Volume 25 (2).

Ravindar R. and V. Sriram, 2021, Impact Pressure and Forces on a Vertical Wall with Different Types of Parapet, Journal of Waterway, Port, Coastal, and Ocean Engineering, 147 (3).

Romano, A., Bellotti, G. Briganti, R. and L. Franco, 2015. Uncertainties in the physical modelling of the wave overtopping over arubble mound breakwater: The role of the seeding number and of thetest duration, Coastal Engineering, 103, 15-21.

Schüttrumpf H., Oumeraci, H. Layer thicknesses and velocities of wave overtopping flow at sea dikes, Coastal Engineering 2005, 52 (6), 473-495.

Smolka, E., Zarranz, G., Medina, J.R., 2009. Estudio Experimental del Rebase de un Dique en Talud de Cubípodos (in Spanish). In: X Jornadas Espa~nolas de Costas y Puertos (Universidad de Cantabria-Adif Congresos), pp. 803–809 (in Spanish).

Stagonas, D., Warbrick, D., Muller G., Magagna D., 2011. Surface tension effects on energy dissipation by small scal, experimental breaking waves, Coastal Engineering 58, 826-836.

Touili, N., Baztan, J., Vanderlinden, J.P., Kane, I.O., Diaz-Simal, P., Pietrantoni, L., et al., 2014. Public perception of engineering-based coastal flooding and erosion risk mitigation options: Lessons from three European coastal settings. Coastal Engineering 87, 205–209.

Van der Meer, J.W., Verhaeghe, H., Steendam, G.J., 2009. The new wave overtopping database for coastal 357 structures. Coastal Engineering 56, 108–120.

Van der Meer, J.W and Bruce, T., 2014. New Physical Insights and Design Formulas on Wave Overtopping at Sloping and Vertical Structures, Journal of Waterway, Port, Coastal, and Ocean Engineering, 140.

Van Doorslaer, K., De Rouck, J., Audenaert, S. and Duquet, V., 2015a. Crest modifications to reduce wave overtopping of non-breaking waves over a smooth dike slope, Coastal Engineering 101, 69-88.

Van Doorslaer K., Romano A., Bellotti G., Altomare C., Cáceres I., De Rouck J., Franco L. and van der Meer, J.W., 2015b. Force Measurements on Storm Walls Due to Overtopping Waves: A Middle-Scale Model Experiment, Proc. of Coastal Structures and Solutions to Coastal Disasters Joint Conference 2015, https://ascelibrary.org/doi/pdf/10.1061/9780784480304.069

Van Doorslaer K., Romano A., De Rouck J. and Kortenhaus A., 2017. Impacts on a storm wall caused by non-breaking waves overtopping a smooth dike slope, Coastal Engineering 120, 93-111.

Van Doorslaer, K. 2018. Reduction of wave overtopping by and wave-induced forces on storm walls and promenades at crest level of smooth dikes : an experimental study, PhD thesis, University of Ghent.

Van Gent M.R.A., Van den Boogaard H.F.P., Pozueta B., Medina J.R., 2007, Neural network modelling of wave overtopping at coastal structures, Coastal Engineering 54, 586–593.

Van Gent, M.R.A., Van der Werf, I.M., 2019. Influence of oblique wave attack on wave overtopping and forces on rubble mound breakwater crest walls, Coastal Engineering 151, 78-96.

Wang, S., 1974. Plunger-type wavemakers: theory and experiment. Journal of Hydraulic Research, 12 (3), 357–388.

Woodruff, J.D., Irish, J.L., Camargo, S.J., 2013. Coastal flooding by tropical cyclones and sea-level rise, Nature, 504(7478), pp. 44-52.

Zanuttigh B., Simcic D., Bagli S., Bozzeda F., Pietrantoni L., Zagonari F., Hoggart S., Nicholls R. J.,2014a. THESEUS decision support system for coastal risk management, Coastal Engineering, 87, 218-239, Elsevier, http://dx.doi.org/10.1016/j.coastaleng.2013.11.013.

Zanuttigh, B., van der Meer, J. W., Bruce, T. & S. Hughes, 2014b. Statistical characterization of extreme overtopping volumes, Proc. ICE 2013, From Sea to Shore – Meeting the challenges of the sea, 442-451, ISBN 978-0-7277-5975-7, ICE publishing.

Zanuttigh B., Formentin S.M., and van der Meer., J.W., 2016. Prediction of extreme and tolerable wave overtopping discharges through an advanced neural network, Ocean Engineering, 127, 7-22.

Zanuttigh B. and Formentin S.M., 2018. Reduction of the wave overtopping discharge at dikes in presence of crown walls with parapets, in: Proceedings of 36th ICCE, Baltimore (MD), 2018.

Zelt, J.A., Skjelbreia, J.E., 1992. Estimating incident and reflected wave field using an arbitrary number of wave gauges. Proc. 23rd ICCE, Venice (I), vol. I, 777–789.